Monograph:
Morris, A.S. and Madani, A. (1995) Quadratic Optimal Control of a Two Flexible-Link Robot Manipulator. Research Report. ACSE Research Report 590 . Department of Automatic Control and Systems Engineering

---

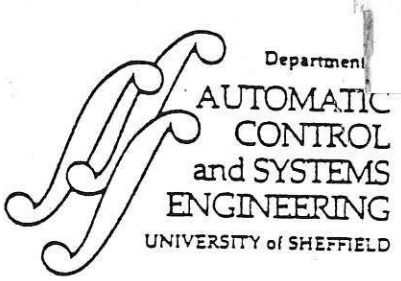

QUADRATIC OPTIMAL CONTROL OF A TWO-FLEXIBLE-LINK ROBOT MANIPULATOR

A. S. MORRIS and A. MADANI

Robotics Research Group,

Department of Automatic Control and Systems Engineering,

The University of Sheffield, Mappin Street, Sheffield, S1 3JD, United Kingdom.

RESEARCH REPORT NUMBER 590

24 July 1995

Tel : +44 (0)114 2825250
Fax : +44 (0)114 2731729
EMail : rrg@sheffield.ac.uk
Robotics Research Group

QUADRATIC OPTIMAL CONTROL OF A TWO-FLEXIBLE-LINK ROBOT MANIPULATOR

by

A. S. Morris, BEng, PhD, CEng, MIEE, MInstMC and A. Madani, BEng

Abstract—This paper is addressed at the problem of controlling a two-flexible-link manipulator system. Manipulators with some flexible links are attractive if high speed motion is required in manufacturing operations because they avoid the severe control problems associated with the large inertia forces generated when the large-mass, rigid links in conventional robot manipulators move at high speed. In fact, only two of the links within a typical six degrees of freedom revolute-geometry industrial robot cause significant inertia forces, and so only these two links need to be flexible. The development of a two-flexible-link system controller is therefore very relevant to larger manipulators, because it can be readily expanded by adding simple controllers for the other rigid links. Two alternative controllers are developed in this paper, a computed-torque controller and a quadratic optimal controller. Simulations confirm the superior performance of the latter.

1 INTRODUCTION

With the increasing demand for faster robot movements in manufacturing operations, there is now widespread interest in developing low-mass, flexible-link robot manipulators which avoid the severe control problems caused by the large inertia forces generated when the large-mass, rigid links associated with conventional robot manipulators move at high speed. Unfortunately, using flexible links instead of rigid ones does not elimate the control problem but only changes it: instead of on-line compensation for inertia forces in a rigid-link robot, the flexible-manipulator controller has to respond to link flexure and the consequent vibrations.

The necessary pre-requisite for a flexible manipulator controller is the existence of a suitably-accurate model of the manipulator system. In practice, a typical revolute-geometry industrial robot manipulator has six degrees of freedom but the problematical inertia forces are due to just two of the links within it. Thus, it will normally only be necessary to have a manipulator with two flexible links to avoid large inertia forces and the ensuing control problems: all other links can remain rigid. Hence, the necessary manipulator model can be divided into two connected sub-systems: a two-flexible-link model and a model of the other rigid links. The detailed development of a two-flexible-link system model has been described previously [1] and [2], and so, only an overview is presented in this paper. The method of approach is to develop an accurate single-flexible-link model and then to expand this into a two-flexible-link model, taking proper account of the coupling and interactions between the two links. Because of this coupling and the fact that errors are consequently cumulative, it is essential that the basic single-link model on which the two-link model is built is of very high accuracy.

The controller of a flexible manipulator system must fulfil two functions. Firstly, it must compensate for the static deflection of the flexible links under gravity forces and, secondly, it must act to reduce both the magnitude and time duration of link oscillations which arise naturally out of its flexibility. A computed-torque controller is able to fulfil both of these functions to a limited extent, but simulations comparing its performance with that of a quadratic optimal controller confirm the superior performance of the latter.

2 MODEL FOR A SINGLE FLEXIBLE LINK

The assumed mode method (AMM) is a computationally efficient scheme which serves as a useful starting point in formulating a flexible link model. Assuming the magnitude of flexure to be low, the

slope and static deflection of a flexible beam bending under gravity are described by:

$$\frac{du_m}{dx} = -\frac{mg}{2EIl}\left(l^2x - lx^2 + \frac{x^3}{3}\right) \; ; \quad u_m = -\frac{mg}{2EIl}\left(\frac{l^2x^2}{2} - \frac{lx^3}{3} + \frac{x^4}{12}\right) \tag{1}$$

where m is the mass of the beam, l is the length of the beam, EI is the flexural stiffness of the beam, g is the gravity vector, x is the position on the beam of the point where the slope and deflection is measured and the subscript m denotes the slope or deflection resulting from the mass of the beam.

For a flexible link with an end-tip load m_t (Figure 1(a)), the mass m_t produces a negative slope and deflection given by:

$$\frac{du_{m_t}}{dx} = -\frac{m_t g}{EI}\left(lx - \frac{x^2}{2}\right) \; ; \quad u_{m_t} = -\frac{m_t g}{EI}\left(\frac{lx^2}{2} - \frac{x^3}{6}\right) \tag{2}$$

By the principle of superposition the total static slope and deflection for a flexible link are given by:

$$\frac{du}{dx} = \frac{du_m}{dx} + \frac{du_{m_t}}{dx} = -\frac{g}{2EIl}\left((m+2m_t)l^2x - (m+m_t)lx^2 + \frac{mx^3}{3}\right)$$

$$u = u_m + u_{m_t} = -\frac{g}{2EIl}\left((m+2m_t)\frac{l^2x^2}{2} - (m+m_t)\frac{lx^3}{3} + \frac{mx^4}{12}\right) \tag{3}$$

The maximum static slope and deflection of the flexible link occur at the free end, where $x = l$, i.e.

$$\frac{du_{max}}{dx} = -\frac{l^2 g}{2EI}\left(\frac{m}{3} + m_t\right) \; ; \quad u_{max} = -\frac{l^3 g}{2EI}\left(\frac{m}{4} + \frac{2m_t}{3}\right) \tag{4}$$

The deflection of the link end-tip is calculated in the above equations on the assumption that the end-tip moves vertically downwards instead of in a circular arc. This is clearly only valid if the magnitude of flexure is low. This condition is unlikely to be satisfied in typical industrial flexible manipulator links, and modification of the equations is therefore necessary.

Previous work [1] has shown that the case of large magnitude flexure can be handled by adding a correction factor to the basic equations. This is calculated by considering the link as a body composed of n equal sections and applying finite element analysis.

The corrected coordinates of the end-tip are then given in [1] and [2] by:

$$x_e = l - s \qquad \text{and} \qquad y_e = u(l-s) \tag{5}$$

where:

$$s = \sum_{i=1}^{n-1} w_i \tag{6}$$

$$v_n = L - l/n \; ; \qquad w_n = \frac{v_n l}{nL} \; ; \qquad L = \sqrt{(u(l-s) - u((n-1)l/n - s))^2 + (l/n)^2} \tag{7}$$

$$u(l - s - w_n) = \frac{w_n}{v_n}\, u(l-s) \tag{8}$$

2.1 DYNAMIC MODELLING

The equation of motion of an undamped flexible link without payload is described by [3] and [4]:

$$\rho\frac{\partial^2 u(x,t)}{\partial t^2} = -\frac{\partial^2}{\partial x^2}\left(EI\frac{\partial^2 u(x,t)}{\partial x^2}\right) \; ; \qquad u(x,t) = \phi(x)q(t) \tag{9}$$

where ρ is the mass per unit length of the link, $u(x,t)$ is the deflection of the link, $\phi(x)$ is the assumed mode shape function and $q(t)$ is the modal function. Assuming that EI is a constant, allows Eq. (9) to be written as

$$\frac{1}{q(t)}\frac{d^2q(t)}{dt^2} = -\frac{EI}{\rho}\frac{1}{\phi(x)}\frac{d^4\phi(x)}{dx^4} \tag{10}$$

which leads to the two following differential equations:

$$\frac{d^4\phi(x)}{dx^4} - \beta^4\phi(x) = 0 \; ; \qquad \frac{d^2q(t)}{dt^2} + \omega^2 q(t) = 0 \tag{11}$$

where w is a constant and $\beta^4 = \rho\omega^2/EI$.
The solution as found in [3] and [4] is:

$$\phi_i(x) = C_i(\cos\beta_i x - \cosh\beta_i x) + (\sin\beta_i x - \sinh\beta_i x) \tag{12}$$

and

$$q_i(t) = A_i\cos\omega_i t + B_i\sin\omega_i t \tag{13}$$

where A_i, B_i, C_i and ω_i are constants, i denotes the number of modes of vibration. The deflection is then given by

$$u(x,t) = \sum_{i=1}^{\infty}\phi_i(x)q_i(t) \tag{14}$$

From the boundary conditions ($u(0,t) = u(l,t) = \frac{\partial u}{\partial x}(0,t) = \frac{\partial^2 u}{\partial x^2}(l,t) = 0$) we obtain

$$C_i = \frac{\cos\ \beta_i l + \cosh\ \beta_i l}{\sin\ \beta_i l - \sinh\ \beta_i l} \tag{15}$$

and β_i as a solution to

$$\cos\ \beta_i l\ \cosh\ \beta_i l = -1 \tag{16}$$

Solving Eq. (16) for the first four modes gives $\beta_1 l = 1.875$, $\beta_2 l = 4.694$, $\beta_3 l = 7.854$ and $\beta_4 l = 10.995$. From here, using the definition that $\beta_i^4 = \rho\omega_i^2/EI$, we can deduce the values of the natural frequencies ω_i of the flexible link for the first four modes. This means that, given an initial excitation F, the link is going to oscillate according to a combination of these four natural frequencies.

The equation of motion can be generalised as an eigenvalue problem linking the two parts of the system (the assumed mode shape functions $\phi_i(x)$ and the modal functions $q_i(t)$). Subsequent analysis [1] taking into account the first three modes (i =1,2 and 3) leads to the following equations for the vertical displacement $u(x,t)$ of any point x on the link at any time t, the slope $u'(x,t)$ of the link at any point x and any time t and the velocity $\dot{u}(x,t)$ of any point x on the link at any time t:

$$u(x,t) = \phi_1(x)q_1(0)\cos\omega_1 t + \phi_2(x)q_2(0)\cos\omega_2 t + \phi_3(x)q_3(0)\cos\omega_3 t \tag{17}$$

$$u'(x,t) = \frac{\partial u(x,t)}{\partial x} = \phi_1'(x)q_1(0)\cos\omega_1 t + \phi_2'(x)q_2(0)\cos\omega_2 t + \phi_3'(x)q_3(0)\cos\omega_3 t \tag{18}$$

$$\dot{u}(x,t) = \frac{\partial u(x,t)}{\partial t} = -\phi_1(x)q_1(0)\omega_1\sin\omega_1 t - \phi_2(x)q_2(0)\omega_2\sin\omega_2 t - \phi_3(x)q_3(0)\omega_3\sin\omega_3 t \tag{19}$$

subject to the initial conditions:

$$u(x,0) = \sum_{i=1}^{\infty}\phi_i(x)q_i(0) = f(x) \; ; \qquad \dot{u}(x,0) = \sum_{i=1}^{\infty}\phi_i(x)\dot{q}_i(0) = g(x) \tag{20}$$

Using the orthogonal relation, the corresponding initial conditions in the *normal coordinates* (the normalisation or weighting is operated on all modes) are

$$q_i(0) = \frac{\rho l}{m_{ii}}\int_0^l f(x)\phi_i(x)dx \; ; \qquad \dot{q}_i(0) = \frac{\rho l}{m_{ii}}\int_0^l g(x)\phi_i(x)dx \tag{21}$$

Similarly, $q_i(0)$ and $\dot{q}_i(0)$ can be obtained from the normalised flexural stiffness as

$$q_i(0) = \frac{EI}{k_{ii}} \int_0^l f''(x)\phi_i''(x)dx \; ; \qquad \dot{q}_i(0) = \frac{EI}{k_{ii}} \int_0^l g''(x)\phi_i''(x)dx \tag{22}$$

When an end-tip load is added to the link, an extra eigenvalue will appear in the boundary conditions and it can be shown [1] and [2] that the effect is to cause the link to vibrate at a slower frequency and for vibrations to persist for a longer period of time.

2.2 INCLUSION OF SHEAR DEFORMATION EFFECT

The assumed mode method neglects shear deformation effects and calculates link deformation on the assumption that this is due only to the bending moment created by the mass and end-tip load of the link. This assumption appears to have been made in all flexible link models previously reported. However, a shear force also exists which acts in the opposite direction to the bending moment and produces motion which has been shown to be significant [5]. Thus, in the interests of accurate modelling, the shear deformation effect must be included in both static and dynamic models of a flexible link.

It is known that the shear force of flexible arms depends on the shape of the cross-section of the arm. Therefore, a physical quantity called the *numerical factor*, representing the geometric characteristics of the link cross-section, is required in the dynamic formulation of the manipulator.

Referring to [6], the numerical factor of a flexible beam is defined as

$$K = \frac{AQ}{I_a d} \tag{23}$$

where, I_a is the moment of inertia of the cross-sectional shape of the link computed with respect to its neutral axis, Q denotes the first moment about the neutral axis of the area contained between an edge of the cross-section of the beam parallel to the main axis and the surface at which the shear stress is to be computed, A is the cross-sectional area and d is the width of the cross-sectional area at which the shear deformation is required. For a uniform link of square cross section, the factor K is given by:

$$K = \frac{AQ}{I_a d} = \frac{d^2(\rho l)l^2/2}{(\rho l)l^2 d/3} = \frac{3d}{2} \tag{24}$$

An element dx of the flexible link is deformed by the shear force V and the bending moment M shown in Figure 1(b). When the shear force is zero, the centre line of dx is normal to the face of the cross-section. If $\partial u(x,t)/\partial x$ is the slope due to the bending moment M, neglecting the interaction between the shear and the moment, the shear force will cause a rectangular element to become a parallelogram without a rotation of the faces.

Thus, the slope of the deflection curve is decreased by the shear angle as formulated in the following equation:

$$\frac{\partial u_c(x,t)}{\partial x} = \frac{\partial u(x,t)}{\partial x} - \frac{V}{KAG} \tag{25}$$

where V is the value of the shear force and is equal to $EI\rho$, G the shear modulus of the material the link is made of and $\partial u_c/\partial x$ the total slope cause by both shear and moment.

As a result of the above formulation, the equation of motion of an undamped flexible link after addition of the shear deformation becomes

$$EI\frac{\partial^4 u_c}{\partial x^4} + \rho\frac{\partial^2 u_c}{\partial t^2} - \frac{EI\rho}{KAG}\frac{\partial^4 u_c}{\partial x^2 \partial t^2} = 0 \tag{26}$$

This equation is very difficult to solve because of the last term in the left hand-side. However, supposing that the shear force affects only the modal functions $q_i(t)$, a solution is found in [7] as being

$$\phi_i(x) = A_i(\cos\beta_i x - \cosh\beta_i x) + \sin\beta_i x - \sinh\beta_i x \tag{27}$$

and

$$q_{ci}(t) = q_{ci}(0)\cos(\omega_{ci}t + \psi) \tag{28}$$

where β_i are obtained in the same manner as for the system without shear deformation, (i.e., as in section 2.1) and ω_{ci} are the transformed natural frequencies including the shear deformation and are given by

$$\omega_{ci} \simeq \omega_i \left[1 - \frac{1}{2}\frac{EI}{KAG}\beta_i^2\right] \tag{29}$$

ω_i being the natural frequencies of the system without shear deformation.
The angle ψ is equal to

$$\psi = \frac{V}{KAG} = \frac{EI\rho}{KAG} \tag{30}$$

From this set of equations, we can see how the shear deformation decreases the natural frequencies of vibration of the link. The effect is more pronounced for the higher modes because of the existence of the term β_i^2 in the equation for ω_{ci}. The total slope is also decreased by the amount ψ. Thus it is apparent that the shear deformation acts similarly to a load on the frequency of the system, but operates in the opposite manner for the slope.

3 EXTENSION OF MODEL TO TWO-FLEXIBLE-LINK SYSTEM

The main difficulty in modeling multi-link flexible manipulators is that the rigid motion and the elastic motion are coupled together, and the elastic motion has direct effects on the transformation matrix between the link coordinates and the global coordinates. Due to the complexity of the problem, the modeling of flexible manipulators is initially simplified by neglecting the effect of the elastic motion on the transformation matrix and neglecting the effect of the elastic motion on the rigid motion.

If the rigid motion is not affected by the elastic motion, the rigid system dynamic equations can be derived using the Lagrange-Euler principle. These equations can then be used to predict the dynamic stress and elastic deformation of the system, by applying the respective torques obtained for the rigid motion to the dynamic equations describing the elastic motion. For the two-link flexible case, this is difficult because of the cross-interaction between the two links. The task of modeling a two-link flexible manipulator is made even harder by the fact that this cross-interaction between the two links is permanently present, i.e., a small disturbance at the end-tip of the first link will cause this link to start a vibrational motion, causing the second link to engage in a motion that will affect the vibrational motion of the first link, and so on ...

To avoid this problem and simplify the modeling of a two-link flexible manipulator without compromising on accuracy, the first type of cross-interaction will be ignored, by assuming that any energy produced in the second link is absorbed through the actuator of this link and therefore cannot propagate to the first link. Thus, the following modelling methodology can be applied:

1. Define the equations of motion for the rigid motion by formulating the necessary torques that are going to be applied to the respective actuators either by choosing the appropriate angles of rotation θ_i, or by using the initial cartesian and desired cartesian coordinates of the manipulator.
2. Define the set of dynamic equations for the flexible motion (only the flexible modes are included in this formulation). From here, a state-space representation of the flexible system can be sought in order to study the elastic behaviour of each link.
3. Apply the desired torques to the flexible system.
4. Implement the Correction Factor in the response.

5. Combine the two motions (rigid and elastic) according to the principle of superposition and deducing the general motion of the manipulator.

This modelling methodology for the elastic motion has been further simplified by the use of only the first three flexible modes, since higher modes have negligible influence on the behaviour of the system [1] and [5].

The full derivation of the two-flexible-link system model is given in [2], and only a summary of this is provided below:

The rigid motion of a two-link manipulator can be described in terms of the Lagrange-Euler formulation:

$$\frac{d}{dt}\left[\frac{\partial L}{\partial \dot{\theta}_i}\right] - \frac{\partial L}{\partial \theta_i} = \tau_i \qquad i = 1, 2. \tag{31}$$

where L is the Lagrangian function and is equal to $K - P$, K is the total kinetic energy of the robot arm, P is the total potential energy of the robot arm, θ_i are the angular joint positions, τ_i are the generalised torques applied to the system at joint i to drive link i as defined in:

$$\tau_i = \sum_{k=1}^{n} D_{ik}\ddot{\theta}_k + \sum_{k=1}^{n}\sum_{m=1}^{n} h_{ikm}\dot{\theta}_k\dot{\theta}_m + c_i \qquad i = 1, 2. \tag{32}$$

or in a matrix form as

$$\tau(t) = D(\theta(t))\ \ddot{\theta}(t) \ + \ h(\theta(t), \dot{\theta}(t)) \ + \ c(\theta(t)) \tag{33}$$

where $\tau(t)$ is a 2×1 generalised torque vector applied at joints $i = 1, 2$.
$\theta(t)$ is a 2×1 vector of the joint positions,
$\dot{\theta}(t)$ is a 2×1 vector of the joint velocities,
$\ddot{\theta}(t)$ is a 2×1 vector of the joint accelerations,
$D(\theta)$ is a 2×2 inertial acceleration-related symmetric matrix.

3.1 WORK SPACE

For a two-link rigid manipulator operating in the vertical plane, the work space is a circle of radius equal to the sum of the lengths of the two rigid links. If the links are flexible, the radius of the circle is reduced by link flexure and becomes a function of the length, width, stiffness, mass and loading of each link. To determine the value of the radius of the circle of influence of a two-link flexible manipulator, it is necessary to first determine the static deflections at the end-tip of each of the links, then obtain the value of the horizontal deformations associated with these deflections. The static deflection at the end-tip of the second link is given by

$$u_2(l) = -\frac{l^3 g}{2EI}\left(\frac{m_2}{4} + \frac{2m_t}{3}\right) \tag{34}$$

where m_2 is the mass of the second link and m_t is the mass of the payload.
The static deflection at the end-tip of the first link is given by

$$u_1(l) = -\frac{l^3 g}{2EI}\left(\frac{m_1}{4} + \frac{2(m_t + m_2 + m_m)}{3}\right) \tag{35}$$

where m_1 is the mass of the first link and m_m is the mass of the actuator for the second link considered to be a part of the payload for the first link. The two links are considered to have the same length l and the same stiffness EI.

Using the correction factor, the static deflections at both end-tips are corrected and the horizontal projections (L_1' and L_2') of the deformed links are calculated. The maximum reach (L_i) for each link is deduced from the following equation:

$$L_i = \sqrt{(L_i')^2 + (u_{ic}(l))^2} \qquad i = 1, 2. \tag{36}$$

where the subscript c denotes that the correction factor has been applied to the variable. The radius of the circle of influence of a two-link flexible manipulator is therefore

$$R = L_1 + L_2 \tag{37}$$

3.2 STATE-SPACE REPRESENTATION OF THE FLEXIBLE SYSTEM

The equation of elastic motion of a flexible link which is part of a multi-link system can be written as (see [1], [3] and [4]):

$$u_j(x,t) = \sum_{i=1}^{n} \phi_{ij}(x) q_{ij}(t) \tag{38}$$

where the subscript j denotes the link number ($j = 1$ for the first link),the subscript i denotes the mode number, $u_j(x,t)$ is the vertical deflection of the link j at the distance x and time t, $\phi_{ij}(x)$ is a shape function defined in [3] and [4], and $q_{ij}(t)$ is a modal function solution of the following second order differential equation:

$$\frac{d^2 q_{ij}(t)}{dt^2} + \frac{c_j}{m_{ij}} \frac{dq_{ij}(t)}{dt} + \omega_{ij}^2 q_{ij}(t) = \tau_j(t) \tag{39}$$

where c_j is the damping coefficient of the link, m_{ij} is the normalised mass for each mode i of the link j and ω_{ij} is the corresponding frequency equal to $\sqrt{k_{ij}/m_{ij}}$, k_{ij} being the normalised stiffness of the ith mode of the jth link.

Typically, the contributions of the flexible modes attenuate rapidly with frequency such that it is always possible to characterise the system dynamics to any required degree of accuracy with only a finite number of the lower modes. Considering only the first three flexible modes of each link, the flexible system can be described in the following state variable form:

$$\begin{Bmatrix} \dot{q}_{1j} \\ \ddot{q}_{1j} \\ \dot{q}_{2j} \\ \ddot{q}_{2j} \\ \dot{q}_{3j} \\ \ddot{q}_{3j} \end{Bmatrix} = \begin{bmatrix} 0 & 1 & 0 & 0 & 0 & 0 \\ -\omega_{1j}^2 & -\frac{c_j}{m_{1j}} & 0 & 0 & 0 & 0 \\ 0 & 0 & 0 & 1 & 0 & 0 \\ 0 & 0 & -\omega_{2j}^2 & -\frac{c_j}{m_{2j}} & 0 & 0 \\ 0 & 0 & 0 & 0 & 0 & 1 \\ 0 & 0 & 0 & 0 & -\omega_{3j}^2 & -\frac{c_j}{m_{3j}} \end{bmatrix} \begin{Bmatrix} q_{1j} \\ \dot{q}_{1j} \\ q_{2j} \\ \dot{q}_{2j} \\ q_{3j} \\ \dot{q}_{3j} \end{Bmatrix} + \begin{bmatrix} 0 \\ b_{1j} \\ 0 \\ b_{2j} \\ 0 \\ b_{3j} \end{bmatrix} \tau_j(t)$$

and with the position vector given by:

$$u_j(x,t) = [\phi_{1j}(x)\ 0\ \phi_{2j}(x)\ 0\ \phi_{3j}(x)\ 0][q_{1j}\ \dot{q}_{1j}\ q_{2j}\ \dot{q}_{2j}\ q_{3j}\ \dot{q}_{3j}]^T \tag{40}$$

This description can also be expressed in the following simplified form:

$$\begin{cases} \dot{q}_j = A_j\ q_j + B_j\ \tau_j \\ u_j(x) = C_j(x)\ q_j \end{cases} \tag{41}$$

The constants b_{ij} are obtained after normalisation of the torques τ_j for each mode of the flexible link j. The state-space representation given by Eqs. (40) is incomplete without the initial conditions relating to each link such as static deflection, relative position of each link in the reference frame and effect of the first link on the second link. These points will be discussed in the next sections by studying each link separately.

3.2.1 Link 1

According to Eqs. (40), the elastic motion of the first flexible link can be described by the following state-space representation:

$$\begin{Bmatrix} \dot{q}_{11} \\ \ddot{q}_{11} \\ \dot{q}_{21} \\ \ddot{q}_{21} \\ \dot{q}_{31} \\ \ddot{q}_{31} \end{Bmatrix} = \begin{bmatrix} 0 & 1 & 0 & 0 & 0 & 0 \\ -\omega_{11}^2 & -\frac{c_1}{m_{11}} & 0 & 0 & 0 & 0 \\ 0 & 0 & 0 & 1 & 0 & 0 \\ 0 & 0 & -\omega_{21}^2 & -\frac{c_1}{m_{21}} & 0 & 0 \\ 0 & 0 & 0 & 0 & 0 & 1 \\ 0 & 0 & 0 & 0 & -\omega_{31}^2 & -\frac{c_1}{m_{31}} \end{bmatrix} \begin{Bmatrix} q_{11} \\ \dot{q}_{11} \\ q_{21} \\ \dot{q}_{21} \\ q_{31} \\ \dot{q}_{31} \end{Bmatrix} + \begin{bmatrix} 0 \\ b_{11} \\ 0 \\ b_{21} \\ 0 \\ b_{31} \end{bmatrix} \tau_1(t)$$

where

$$m_{i1} = \int_0^l [\rho + m_l \delta(x-l)] \phi_{i1}^2 dx \qquad i = 1, 2, 3. \tag{42}$$

m_l being the mass of the payload for the first link which consists of the mass m_a of the actuator of the second link, the mass ρl of the second link and the mass m_t of the payload at the end-tip of the second link.

The normalised flexural stiffness k_{i1} relative to each mode is given by

$$k_{i1} = \int_0^l EI(\phi_{i1}'')^2 dx \qquad i = 1, 2, 3. \tag{43}$$

The constants b_{i1} are deduced from the normalisation of the principal torque $\tau_1(t)$ applied to the link, and are equal to

$$b_{i1} = -\frac{\phi_{i1}(l)}{k_{i1}} \tag{44}$$

The position vector giving the deflection of the link at any point x is

$$u_1(x,t) = [\phi_{11}(x)\ 0\ \phi_{21}(x)\ 0\ \phi_{31}(x)\ 0][q_{11}\ \dot{q}_{11}\ q_{21}\ \dot{q}_{21}\ q_{31}\ \dot{q}_{31}]^T$$

This vector is increased by a value $u_{01}(x)$ corresponding to the static deflection caused by the mass of the link itself and the load attached to its end-tip. So, the deflection vector becomes:

$$u_1(x,t) = [\phi_{11}(x)\ 0\ \phi_{21}(x)\ 0\ \phi_{31}(x)\ 0][q_{11}\ \dot{q}_{11}\ q_{21}\ \dot{q}_{21}\ q_{31}\ \dot{q}_{31}]^T + u_{01}(x) \tag{45}$$

with

$$u_{01}(x) = -\frac{g}{2EIl}\left((\rho l + 2m_l)\frac{l^2x^2}{2} - (\rho l + m_l)\frac{lx^3}{3} + \frac{\rho l x^4}{12}\right) \tag{46}$$

The motion of the first link can be obtained from the inverse Laplace transform of the following equation:

$$u_1(x,s) = C_1(x)(sI - A_1)^{-1} B_1\ \tau_1(s) + u_{01}(x) \tag{47}$$

where s is the Laplace operator and I the identity matrix.

To determine the deflection u_1 at the end-tip of the first link, the variable x is replaced in Eq. (47) by l. The limitation of this state-space representation is that the response $u_1(x,t)$ will be relatively correct only for very small deflections. Since a good accuracy in determining the position of the end-tip of the first link is needed to locate the origin of the second link, the necessity in using the correction factor arises once again. The difficulty in using the correction factor lays in the fact that, unlike the normal procedure required by the state-space representation where the variable x is replaced by the value at which the deflection of the link is wanted (for this case x=l), the Correction Factor Method requires the value of the deflection all along the link. In order to obtain a good accuracy, the incrementation of the variable x has to be very small (independently from the number of finite elements chosen to approximate the flexible link). All this generates some extensive calculation and increases the computing time needed to obtain a response for the corrected deflection.

3.2.2 Link 2

In the same manner as for the first link, the equations governing the elastic motion of the second link can be structured in a state-space representation as:

$$\begin{Bmatrix} \dot{q}_{12} \\ \ddot{q}_{12} \\ \dot{q}_{22} \\ \ddot{q}_{22} \\ \dot{q}_{32} \\ \ddot{q}_{32} \end{Bmatrix} = \begin{bmatrix} 0 & 1 & 0 & 0 & 0 & 0 \\ -\omega_{12}^2 & -\frac{c_2}{m_{12}} & 0 & 0 & 0 & 0 \\ 0 & 0 & 0 & 1 & 0 & 0 \\ 0 & 0 & -\omega_{22}^2 & -\frac{c_2}{m_{22}} & 0 & 0 \\ 0 & 0 & 0 & 0 & 0 & 1 \\ 0 & 0 & 0 & 0 & -\omega_{32}^2 & -\frac{c_2}{m_{32}} \end{bmatrix} \begin{Bmatrix} q_{12} \\ \dot{q}_{12} \\ q_{22} \\ \dot{q}_{22} \\ q_{32} \\ \dot{q}_{32} \end{Bmatrix} + \begin{bmatrix} 0 \\ b_{12} \\ 0 \\ b_{22} \\ 0 \\ b_{32} \end{bmatrix} \tau_2(t)$$

All the constants are determined in the same manner as for the first link.
The position vector giving the deflection at any point x on the link is:

$$u_2(x,t) = [\phi_{12}(x)\ 0\ \phi_{22}(x)\ 0\ \phi_{32}(x)\ 0][q_{12}\ \dot{q}_{12}\ q_{22}\ \dot{q}_{22}\ q_{32}\ \dot{q}_{32}]^T + u_{02}(x) \tag{48}$$

with $u_{02}(x)$ being the value of the static deflection of the link at a distance x from its origin. This static deflection is caused by the mass ρl of the link plus its payload m_t and is equal to

$$u_{02}(x) = -\frac{g}{2EIl}\left((\rho l + 2m_t)\frac{l^2x^2}{2} - (\rho l + m_t)\frac{lx^3}{3} + \frac{\rho l x^4}{12}\right) \tag{49}$$

In a similar manner to that of the first link, the response of the second link can be obtained from the inverse Laplace transform of the following equation:

$$u_2(x,s) = C_2(x)(sI - A_2)^{-1}B_2\ (\tau_1(s) + \tau_2(s)) + u_{02}(x) \tag{50}$$

The next step in the modeling of a two-link flexible manipulator consists of repositioning the origin of the second link. This is done by obtaining the corrected horizontal and vertical positions of the end-tip of the first link and assigning these values to the coordinates of the origin of the second link. Then, the vibration and (or) rotation of the first link is used as an additional input to the second link. This is considered as the effect of the first link on the second link. This operation is carried out by obtaining the time-varying slope $du_1(l,t)/dx$ of the end-tip of the first link through the correction factor method and adding it to the angular position $\theta_2(t)$ of the second link.

3.3 FINAL MODEL

The block diagram in Figure 2 summarises the modelling algorithm for the two-link flexible manipulator. The model is divided into two sub-systems, one for each link. Desired coordinates (x_{1d}, y_{1d}, x_{2d} and y_{2d}) are fed into the system through the block representing the inverse kinematics of the system to generate the desired angles of rotation $\theta_{1d}(t)$ and $\theta_{2d}(t)$. This operation can be omitted if these two desired angles are known initially. Both angles are then used as inputs for the rigid system models representing the two links. Outputs such as link masses, actuator mass, payload, stiffness, length and width of each link, etc., are passed to the second part of each sub-system which computes the elastic motion of each link. Other important outputs produced by each of the two rigid model sub-systems are the applied torques $\tau_1(t)$ and $\tau_2(t)$. Each torque induces the corresponding rigid body to rotate according to the corresponding angle of rotation $\theta_d(t)$ and, simultaneously, provokes a forced vibration into the corresponding flexible sub-system.

The superposition of both motions (rigid and flexible) produces a set of variables for each link; among these are the end-tip vertical positions, the end-tip horizontal positions, the end-tip deflections and the end-tip slopes. Using the Correction Factor Method, all of these outputs are recalculated. As a result, some of them will be used as a feed-back to the whole system to test if the rotations are accomplished, while others (the end-tip slope of link 1, for instance) will be added to the angular position of the rigid body of the second link, therefore quantifying the effect that the first link has on the second link.

4 CONTROLLER DEVELOPMENT

Control techniques for rigid manipulators are now reasonably well developed. Since the dynamics at the hub of such manipulators is the same as the dynamics at the end-tip, the magnitude of the driving torques and forces causing the motion of a rigid manipulator can be used to accurately predict the position of the end-tip at any time. The absence of flexibility enables the manipulator to move without the occurrence of vibrations. Therefore, control techniques are designed to optimise the transition time between the initial position and the desired position of the end-effector.

However, in the case of flexible-link manipulators, the optimisation of the transition time between two positions of the end-point of a flexible manipulator can generate some unwanted characteristics such as vibrations. Depending on the degree of flexibility of the manipulator and the time taken to reach the desired position, the amplitude of these vibrations can be very significant. In consequence, the time gained in increasing the speed of the end-effector between the initial and the final positions may be lost in waiting for the vibrations to settle down.

Early attempts to design an efficient control law that will allow an optimisation of both transition time (fast response) and settling time (decrease of the vibrations) involved linearising the equations of motion of the manipulator about a nominal configuration and applying several linear control schemes [8], [9] and [10], but the lack of accuracy in the model design and the high number of approximations needed in the linearisation produced a system which was far from being realistic.

Shaped torque techniques were proposed by [11] to minimise the residual vibrations in flexible manipulators. This technique has been further developed to suppress multiple mode variations [12]. The computed torque method which was originally developed for rigid manipulators [13] was also tried on flexible link systems. The complexity of the inverse dynamics makes a straightforward application of the computed torque method or feedback linearisation impossible: instead, some approximate schemes are proposed in [14] and [15] for open and closed-loop control. An application of some of these procedures will be looked at in this chapter as a starting point to more elaborate control methods.

The main drawback of all model-based controllers is the difficulty in obtaining the exact model necessary. Therefore, the robustness to parameter uncertainties has been a major concern in control design for flexible manipulators [16]. Another difficulty with the flexible systems is the so called "spillover" problem which occurs when one of the links is vertical. Since the actual system is a distributed parameter system, any designed controller based on finite dimensional models will generally suffer from an inability to control or observe these spillovers [17].

Independent joint PD (proportional plus derivative) controllers have been shown to be stable for rigid manipulators [16]. The same strategy was experimented with on a two-link rigid-flexible manipulator [18] with satisfactory results, but, since their design was based on a linearised model, the manoeuver angles were restricted to small values.

More recent research on one-link flexible manipulators [19] suggested separating the flexible system from the rigid system and controlling the oscillations of the link by the use of quadratic programming. In their model, the absence of analytical equations describing the horisontal oscillations due to the "shrinking" of the link resulted in a large amount of inaccuracies for large manoeuvers. An optimal control procedure based on this method will be presented. Then, the corresponding results will be projected to the two-link flexible manipulator case.

4.1 COMPENSATION FOR THE STATIC DEFLECTION

Before engaging in any trajectory planning, and therefore control strategy, for the two-link flexible manipulator, it is necessary to initially compensate for the two static deflections present at the end-tip of each link. This depends on the link characteristics such as length, cross-sectional area, flexural

stiffness and mass, plus characteristics linked to the payload carried by the link such as its mass and position on the link. A correction procedure was designed to obtain the value of the deflection and the corresponding slope at any point of the link. Then, each link is rotated until its vertical coordinate coincides with the vertical coordinate of its rigid counterpart. In other words, if the rigid body of the manipulator is initially positioned on the horizontal axis ($y_{r1}(l_1,0) = y_{r2}(l_2,0) = 0$, where the subscript r relates to the rigid body), both flexible links are rotated upwards with an angle equal to

$$\phi = -\tan^{-1}\left(\frac{y_{stat1}(l_1)}{x_{stat1}(l_1)}\right) - \tan^{-1}\left(\frac{y_{stat2}(l_2)}{x_{stat2}(l_2)}\right) \tag{51}$$

where the subscript *stat* relates to the end-tip coordinates when subject to static deflection. Results showing the position of a two-link flexible manipulator before and after the compensation has occurred are shown in Figure 3.

4.2 COMPUTED-TORQUE (OPEN-LOOP) CONTROL

Computed torque control is now a well-established open-loop method for rigid manipulators. It can also be extended to flexible manipulators, but careful design is then necessary because of the tendancy of the link end-tip to vibrate with an unacceptable amplitude if the speed of rotation is too high. For this reason, the stability of the open-loop of both flexible subsystems must be carefully analysed.

4.2.1 Open-Loop Stability

Consider the state-space representations, given in [2], describing the two sets of flexible modes:

$$\begin{Bmatrix} \dot{q}_{1j} \\ \ddot{q}_{1j} \\ \dot{q}_{2j} \\ \ddot{q}_{2j} \\ \dot{q}_{3j} \\ \ddot{q}_{3j} \end{Bmatrix} = \begin{bmatrix} 0 & 1 & 0 & 0 & 0 & 0 \\ -\omega_{1j}^2 & -\frac{c_j}{m_{1j}} & 0 & 0 & 0 & 0 \\ 0 & 0 & 0 & 1 & 0 & 0 \\ 0 & 0 & -\omega_{2j}^2 & -\frac{c_j}{m_{2j}} & 0 & 0 \\ 0 & 0 & 0 & 0 & 0 & 1 \\ 0 & 0 & 0 & 0 & -\omega_{3j}^2 & -\frac{c_j}{m_{3j}} \end{bmatrix} \begin{Bmatrix} q_{1j} \\ \dot{q}_{1j} \\ q_{2j} \\ \dot{q}_{2j} \\ q_{3j} \\ \dot{q}_{3j} \end{Bmatrix} + \begin{bmatrix} 0 \\ b_{1j} \\ 0 \\ b_{2j} \\ 0 \\ b_{3j} \end{bmatrix} \tau_j(t) \tag{52}$$

and the position vectors

$$u_j(x,t) = [\phi_{1j}(x)\ 0\ \phi_{2j}(x)\ 0\ \phi_{3j}(x)\ 0]\ [q_{1j}\ \dot{q}_{1j}\ q_{2j}\ \dot{q}_{2j}\ q_{3j}\ \dot{q}_{3j}]^T \tag{53}$$

where $j = 1, 2$ is the link number.
The open-loop transfer function giving the relationship between the input torques $\tau_j(t)$ and the output variables $u_j(x,t)$ can be written as follows:

$$u_j(x,s) = C_j(x)(sI - A_j)^{-1}B_j\ \tau_j(s) + u_{0j}(x) \qquad j = 1,2. \tag{54}$$

where

$$A_j = \begin{bmatrix} 0 & 1 & 0 & 0 & 0 & 0 \\ -\omega_{1j}^2 & -\frac{c_j}{m_{1j}} & 0 & 0 & 0 & 0 \\ 0 & 0 & 0 & 1 & 0 & 0 \\ 0 & 0 & -\omega_{2j}^2 & -\frac{c_j}{m_{2j}} & 0 & 0 \\ 0 & 0 & 0 & 0 & 0 & 1 \\ 0 & 0 & 0 & 0 & -\omega_{3j}^2 & -\frac{c_j}{m_{3j}} \end{bmatrix} \qquad j = 1,2. \tag{55}$$

$$\begin{aligned} B_j &= [0\ b_{1j}\ 0\ b_{2j}\ 0\ b_{3j}]^T \\ &= \left[0\ -\frac{\phi_{1j}(l)}{k_{1j}}\ 0\ -\frac{\phi_{2j}(l)}{k_{2j}}\ 0\ -\frac{\phi_{3j}(l)}{k_{3j}}\right]^T \qquad j = 1,2. \end{aligned} \tag{56}$$

and

$$C_j(x) = [\phi_{1j}(x)\ 0\ \phi_{2j}(x)\ 0\ \phi_{3j}(x)\ 0] \qquad j = 1, 2. \tag{57}$$

Concentrating only on the dynamic response of each subsystem, the corresponding transfer functions can be rewritten as:

$$G_j(x, s) = \frac{u_j(x, s) - u_{0j}(x)}{\tau_j(s)} = C_j(x)(sI - A_j)^{-1}B_j \qquad j = 1, 2. \tag{58}$$

Such open-loop transfer functions for the two links have the poles and seros depicted in Figure 4. The first two elastic modes of each link (marked by a "1" and a "2") produce the most dominant poles (especially for the first link, since the payload is relatively high). The poles of the open-loop for the first link subsystem are -1.12±10.24i, -2.81±52.65i and -7.32±124.33i. While the poles of the open-loop for the second subsystem are evaluated at -2.25±10.06i, -5.62±52.42i and -14.24±123.40i. This proves the dominance of the first and second flexible modes in the response of the system, as well as the stability of both flexible subsystems. It can be seen from the root locii that the dynamic response of both links is mainly dictated by the first modes, since their corresponding poles (in comparison to the other modes) have the smallest real part. This means that the instability of the links is mainly due to their first elastic mode. The settling time for the vibrations is determined by the distance separating each pair of poles. A Nyquist plot (Figure 5) shows the robustness of the open-loop transfer functions. The gain of the transfer function of the first link is obviously more important than that of the second link, proving that the same angle of rotation will produce vibrations of a larger amplitude for the first link, and therefore, a longer settling time.

To achieve the control of the vibrations occurring towards the end of the rotation of each link, a straightforward computed torque technique is derived by producing a smooth trajectory for both flexible links in a way that the energy produced by each torque is conserved, and the rotation time is stretched to an optimal value, therefore limiting the amplitude of the residual vibrations and shortening the settling time for the links to regain their static positions.

4.2.2 Computed Torque Control

Since the relationship between the applied torque τ_j and the dynamic deflection $u_j(x)$ is given by

$$\begin{aligned} u_j(x, s) &= C_j(x)(sI - A_j)^{-1}B_j\ \tau_j(s) + u_{0j}(x) \\ &= G_j(x, s)\tau_j(s) + u_{0j}(x) \qquad j = 1, 2. \end{aligned} \tag{59}$$

$\|G_j(x, i\omega)\|$ being the gain of amplification (i is the complex number), a way of controlling the amplitude of vibration of the links could be obtained by limiting the magnitude of the input τ_j. The control procedure designed involves calculating the torques according to:

$$\begin{bmatrix} \tau_1 \\ \tau_2 \end{bmatrix} = [D(\theta_1, \theta_2)] \begin{bmatrix} \ddot{\theta}_1 \\ \ddot{\theta}_2 \end{bmatrix} + [h(\theta_1, \theta_2, \dot{\theta}_1, \dot{\theta}_2)] + [c(\theta_1, \theta_2)] \tag{60}$$

such that the following conditions are satisfied:

$$\|u_1(x, i\omega)\| \leq \mathcal{L}\{u^d_{1max}(x)\}$$

$$\|u_2(x, i\omega)\| \leq \mathcal{L}\{u^d_{2max}(x)\}$$

where $u^d_{1max}(x)$ and $u^d_{2max}(x)$ are the maximum desired amplitudes for the vibrations at the distance x from the origin of the respective link.
Substituting Eq. (59) in Eq. (60), the control procedure can be formulated as being:

$$\begin{bmatrix} \tau_1 \\ \tau_2 \end{bmatrix} = [D(\theta_1, \theta_2)] \begin{bmatrix} \ddot{\theta}_1 \\ \ddot{\theta}_2 \end{bmatrix} + [h(\theta_1, \theta_2, \dot{\theta}_1, \dot{\theta}_2)] + [c(\theta_1, \theta_2)] \tag{61}$$

such that

$$\|\tau_1(i\omega)\| \leq \mathcal{L}\{u^d_{1max}(x)\} \cdot \|G_1(x, i\omega)\|^{-1}$$

$$\|\tau_2(i\omega)\| \leq \mathcal{L}\{u^d_{2max}(x)\} \cdot \|G_2(x, i\omega)\|^{-1}$$

In order to obtain a dynamic response for the link vibrations within the desired scale set by the maximum desired values $u^d_{1max}(x)$ and $u^d_{2max}(x)$, the respective torques to be delivered to the actuators of both links should satisfy the control condition given by:

$$\|\tau_j(i\omega)\| \leq \mathcal{L}\{u^d_{jmax}(x)\} \cdot \|G_j(x, i\omega)\|^{-1} = \mathcal{L}\{\tau^d_{jmax}\} \qquad j = 1, 2. \tag{62}$$

The aim of this control technique is to find the desired functions giving $\theta_1(t)$ and $\theta_2(t)$ that will produce a smooth trajectory for both end-tips and therefore dampen the residual vibrations of the flexible links.

The nonlinearity of the inverse dynamics equations of the rigid mode make this control procedure very difficult to implement [18]. It can be seen from Eq. (61) that to obtain $\theta_1(t)$ and $\theta_2(t)$ from $\tau_1(t)$ and $\tau_2(t)$ requires parallel programming for a set of highly nonlinear differential equations. A solution adopted was to use a trial and error method, involving setting an initial trajectory for both links, calculating the respective torques, comparing these torques to the conditions provided by the control procedure, then, if the conditions are not satisfied, readjusting the trajectories by increasing the time of rotation.

The results shown in Figures 6 and 7 have been obtained by applying the computed torque technique to the part of the motion when the braking procedure is occurring. The first phase of the motion (acceleration phase) is left intact to optimise on the time criterion. But as soon as the links start to decelerate, the control procedure limits the value of the braking torque to allow a smoother motion, and hence smaller oscillations.

The control procedure shows that the first link rotates at a slower speed than the second link. This is because, to satisfy the conditions listed in Eq. (61), each link has to be rotated according to a specific optimal time dictated by the control law applied on the braking torque. Since the first link is subject to more inertia, its respective time of rotation is increased accordingly.

Figure 6(a) shows that in the absence of any control law, the rigid mode of the first link is rotated by an amount of 30 degrees in 1.18 seconds. After applying a computed torque control on the braking torque relative to the first link, the same rotation is effected in 1.72 seconds. For the second link (see Figure 7(a)), the rigid mode is rotated by an amount of -30 degrees in 1.18 seconds when uncontrolled, and 1.5 seconds when subject to the computed torque control.

Controlling the amplitude of the braking torque, as shown in Figure 8, has obvious repercussions on the response of the end-tip of each link. An uncontrolled link will be subject to a very pronounced braking process, therefore, serious vibrations at the end of the rotation are very likely to occur. The controlled links show an amelioration of the level of amplitude of the residual vibrations, in addition to the fact that the settling time is reduced enormously ($u^d_{1max}(l)$ is set to 24 mm and $u^d_{2max}(l)$ is set to 8 mm).

Finally, the angles of rotation of the uncontrolled, then controlled end-tip of both flexible links are depicted in figure 9. These angles can be compared to those obtained for the rigid mode (Figures 6(a) and 7(a)). The vibrations due to the flexibility of the links are visible, especially towards the end of the manoeuvers. The benefit obtained from applying the computed torque control is also visible, since the oscillations have been dampened and the settling time shortened.

Even though the computed torque control is an efficient method of control for flexible manipulators, the difficulty in solving the highly nonlinear equations describing the inverse dynamics of the system is a very important drawback. The computation burden does not favour an on-line real-time application for this method. As a result, research was directed to closed-loop control and quadratic optimal control in particular.

4.3 QUADRATIC OPTIMAL (CLOSED-LOOP) CONTROL

Given a system described by the following state-space representation:

$$\dot{x} = A\,x + B\,u \tag{63}$$

minimising some function of the error signal will produce the following quadratic performance index:

$$J = \int_0^T [x^d(t) - x(t)]' Q\, [x^d(t) - x(t)]\, dt \tag{64}$$

where $x^d(t)$ represents the desired state, $x(t)$ the actual state (thus, $x^d(t) - x(t)$ is the error vector), Q a positive-definite matrix, and the time interval $0 \leq t \leq T$ is either finite or infinite. The superscript $'$ indicating here the transpose of a vector or matrix.

In addition to considering errors as a measure of system performance, the energy required for the control action is usually added to the performance index. Since the control signal may have the dimension of force or torque, the control energy is proportional to the integral of such control signal squared. If the error function is minimised regardless of the energy required, then a design may result that calls for overly large values of the control signal. This is undesirable since all physical systems are subject to saturation. Large-amplitude control signals are ineffective outside the range determined by saturation. thus, practical considerations place a constraint on the control vector, for example,

$$\int_0^T u'(t) R\, u(t)\, dt = J_R \tag{65}$$

where R is a positive-definite matrix and J_R a positive constant. The performance index of a control system over the time interval $0 \leq t \leq T$ may then be written, with the use of a Lagrange multiplier λ, as

$$J = \int_0^T [x^d(t) - x(t)]' Q\, [x^d(t) - x(t)]\, dt + \lambda \int_0^T u'(t) R\, u(t)\, dt \tag{66}$$

The Lagrange multiplier λ is a positive constant indicating the weight of control cost with respect to minimising the error function. In this formulation $u(t)$ is unconstrained. Design based on this performance index has a practical significance that the resulting system compromises between minimising the integral error squared and minimising the control energy. If $T = \infty$ and the desired state x^d is the origin ($x^d = 0$), then the preceding performance index can be expressed as:

$$J = \int_0^T [x'(t) Q\, x(t) + u'(t) R\, u(t)]\, dt \tag{67}$$

where λ has been included to the matrix R. A choice of weighting matrices Q and R is in a sense arbitrary. Although minimising an "arbitrary" quadratic performance index may not seem to have much significance, the advantage of the quadratic optimal control approach is that the resulting system is a stable system. This approach is sometimes a better alternative to the pole placement approach. The optimisation can also be operated on the output vector ($y(t) = Cx(t)$) instead of the state vector $x(t)$, transforming the performance index into

$$J = \int_0^T [y'(t) Q\, y(t) + u'(t) R\, u(t)]\, dt = \int_0^T [x'(t) C' Q\, Cx(t) + u'(t) R\, u(t)]\, dt \tag{68}$$

4.3.1 State-Controllability

In order to apply a closed-loop control to any dynamic system, the system must satisfy the necessary and sufficient condition that it is completely state controllable. This condition is satisfied when

$$\text{rank}\, [\, B \mid AB \mid \ldots \mid A^{n-1} B\,] = n \tag{69}$$

n being the number of states of the system.
A control law making use of all the states of the system can then be formulated as follows:

$$u(t) = -K\ x(t) \tag{70}$$

where K is the $r \times n$ matrix of the closed-loop gains, or

$$\begin{bmatrix} u_1 \\ u_2 \\ \vdots \\ u_r \end{bmatrix} = - \begin{bmatrix} k_{11} & k_{12} & \dots & k_{1n} \\ k_{21} & k_{22} & \dots & k_{2n} \\ \vdots & \vdots & & \vdots \\ k_{r1} & k_{r2} & \dots & k_{rn} \end{bmatrix} \begin{bmatrix} x_1 \\ x_2 \\ \vdots \\ x_n \end{bmatrix} \tag{71}$$

r being the dimension of the input vector $u(t)$.

4.3.2 Algorithm Development

Considering the case of a two-link flexible manipulator where the state-space representation of the flexible subsystems is given by

$$\begin{Bmatrix} \dot{q}_{1j} \\ \ddot{q}_{1j} \\ \dot{q}_{2j} \\ \ddot{q}_{2j} \\ \dot{q}_{3j} \\ \ddot{q}_{3j} \end{Bmatrix} = \begin{bmatrix} 0 & 1 & 0 & 0 & 0 & 0 \\ -\omega_{1j}^2 & -\frac{c_j}{m_{1j}} & 0 & 0 & 0 & 0 \\ 0 & 0 & 0 & 1 & 0 & 0 \\ 0 & 0 & -\omega_{2j}^2 & -\frac{c_j}{m_{2j}} & 0 & 0 \\ 0 & 0 & 0 & 0 & 0 & 1 \\ 0 & 0 & 0 & 0 & -\omega_{3j}^2 & -\frac{c_j}{m_{3j}} \end{bmatrix} \begin{Bmatrix} q_{1j} \\ \dot{q}_{1j} \\ q_{2j} \\ \dot{q}_{2j} \\ q_{3j} \\ \dot{q}_{3j} \end{Bmatrix} + \begin{bmatrix} 0 \\ b_{1j} \\ 0 \\ b_{2j} \\ 0 \\ b_{3j} \end{bmatrix} \tau_j(t) \tag{72}$$

and the position vectors (or output vectors)

$$u_j(x,t) = [\phi_{1j}(x)\ 0\ \phi_{2j}(x)\ 0\ \phi_{3j}(x)\ 0]\ [q_{1j}\ \dot{q}_{1j}\ q_{2j}\ \dot{q}_{2j}\ q_{3j}\ \dot{q}_{3j}]^T \tag{73}$$

where $j = 1, 2$ is the link number.
The problem of determining the optimal control torques $\tau_j(t)$, $j = 1, 2$, can be solved by minimising the following performance index for each flexible link

$$J_j(x) = \int_0^\infty (u_j'(x,t)Q_j\ u_j(x,t) + \tau_j'(t)R_j\ \tau_j(t))\ dt \quad j = 1, 2. \tag{74}$$

where $u_j(x,t) = C_j(x)\underline{q}_j(x,t)$, $\underline{q}_j(x,t)$ is the vector of state variables of each link at a distance x. Since the control operates on the end-tip response, x is replaced by l. Replacing the torques $\tau_j(t)$ by the feed-back command $-K_j(x)\ \underline{q}_j(x,t)$ gives the new performance index:

$$J_{lj} = \int_0^\infty \underline{q}_{lj}'(t)[C_{lj}'Q_jC_{lj} + K_{lj}'R_jK_{lj}]\underline{q}_{lj}(t)\ dt \quad j = 1, 2. \tag{75}$$

where the subscript lj relates to the end-tip of each flexible link.
The performance index is then solved according to the second method of Liapunov by assuming that

$$\underline{q}_{lj}'(t)[C_{lj}'Q_jC_{lj} + K_{lj}'R_jK_{lj}]\underline{q}_{lj}(t) = -\frac{d}{dt}(\underline{q}_{lj}'(t)P_j\underline{q}_{lj}(t)) \quad j = 1, 2. \tag{76}$$

where P_j is a positive-definite matrix of the form

$$P_j = \begin{bmatrix} p_{j11} & p_{j12} & p_{j13} & p_{j14} & p_{j15} & p_{j16} \\ p_{j12} & p_{j22} & p_{j23} & p_{j24} & p_{j25} & p_{j26} \\ p_{j13} & p_{j23} & p_{j33} & p_{j34} & p_{j35} & p_{j36} \\ p_{j14} & p_{j24} & p_{j34} & p_{j44} & p_{j45} & p_{j46} \\ p_{j15} & p_{j25} & p_{j35} & p_{j45} & p_{j55} & p_{j56} \\ p_{j16} & p_{j26} & p_{j36} & p_{j46} & p_{j56} & p_{j66} \end{bmatrix} \quad j = 1, 2. \tag{77}$$

Eq. (76) can be analytically developed as follows:

$$\begin{aligned}\underline{q}'_{1j}[C'_{1j}Q_jC_{1j}+K'_{1j}R_jK_{1j}]\underline{q}_{1j} &= -\underline{\dot{q}}'_{1j}P_j\underline{q}_{1j}-\underline{q}'_{1j}P_j\underline{\dot{q}}_{1j}\\ &= -\underline{q}'_{1j}[(A_j-B_jK_{1j})'P_j+P_j(A_j-B_jK_{1j})]\underline{q}_{1j}\end{aligned} \tag{78}$$

Comparing both sides of this last equation and noting that this equation must hold true for any $\underline{q}_{1j}$, the requirement becomes

$$(A_j-B_jK_{1j})'P_j+P_j(A_j-B_jK_{1j})=-(C'_{1j}Q_jC_{1j}+K'_{1j}R_jK_{1j}) \tag{79}$$

The second method of Liapunov states that, if $A-BK$ is a stable matrix, there exists a positive-definite matrix P that satisfies the equation above. The performance index can then be evaluated as

$$\begin{aligned}J_{1j} &= \int_0^\infty \underline{q}'_{1j}(t)[C'_{1j}Q_jC_{1j}+K'_{1j}R_jK_{1j}]\underline{q}_{1j}(t)\,dt=-[\underline{q}'_{1j}(t)P_j\underline{q}_{1j}(t)]_0^\infty\\ &= -\underline{q}'_{1j}(\infty)P_j\underline{q}_{1j}(\infty)+\underline{q}'_{1j}(0)P_j\underline{q}_{1j}(0)\end{aligned} \tag{80}$$

Since all the poles of A_j have negative real parts (see section 4.2.1), $\underline{q}_{1j}(\infty)\to 0$, therefore,

$$J_{1j}=\underline{q}'_{1j}(0)P_j\underline{q}_{1j}(0) \qquad j=1,2. \tag{81}$$

Since R_j is assumed to be a positive-definite matrix, it can be written as follows:

$$R_j=T'_jT_j \qquad j=1,2. \tag{82}$$

where T_j is a non-singular matrix. Then Eq. (79) can be written as

$$(A'_j-K'_{1j}B'_j)P_j+P_j(A_j-B_jK_{1j})+C'_{1j}Q_jC_{1j}+K'_{1j}T'_jT_jK_{1j}=0 \tag{83}$$

which can be rewritten as (by definition, $P'_j=P_j$)

$$\begin{aligned}A'_jP_j+P_jA_j &+ [T_jK_{1j}-(T'_j)^{-1}B'_jP_j]'[T_jK_{1j}-(T'_j)^{-1}B'_jP_j]\\ &- P_jB_jR_j^{-1}B'_jP_j+C'_{1j}Q_jC_{1j}=0\end{aligned} \tag{84}$$

The minimisation of J_{1j} with respect to K_{1j} requires the minimisation of

$$\underline{q}'_{1j}[T_jK_{1j}-(T'_j)^{-1}B'_jP_j]'[T_jK_{1j}-(T'_j)^{-1}B'_jP_j]\underline{q}_{1j} \tag{85}$$

with respect to K_{1j}. Since the last expression is nonnegative (a quantity squared), the minimum occurs when it is zero, or when

$$T_jK_{1j}=(T'_j)^{-1}B'_jP_j \qquad j=1,2. \tag{86}$$

Hence

$$K_{1j}=T_j^{-1}(T'_j)^{-1}B'_jP_j=R_j^{-1}B'_jP_j \qquad j=1,2. \tag{87}$$

This last equation gives the optimal matrix K_{1j}. Thus, the optimal control law to the quadratic optimal control problem where the performance index is given by Eq. (74) becomes

$$\tau_j(t)=-K_{1j}\underline{q}_{1j}(t)=-R_j^{-1}B'_jP_j\underline{q}_{1j}(t) \tag{88}$$

The matrix P_j must satisfy Eq. (84) or the following reduced equation:

$$A'_jP_j+P_jA_j-P_jB_jR_j^{-1}B'_jP_j+C'_{1j}Q_jC_{1j}=0 \qquad j=1,2. \tag{89}$$

This equation is called the reduced-matrix Riccati equation. The design steps may be stated as follows:

1. Solve Eq. (89), the reduced-matrix Riccati equation, for the matrix P_j.

2. Substitute this matrix P_j into Eq. (87). The resulting matrix K_{lj} is the optimal feed-back gain.

Since the output to the two flexible subsystems is the deflection at the respective end-tips, Q_j is a scalar used to weight the output $u_{lj}(t)$:

$$Q_j = \mu_j \qquad j = 1, 2. \tag{90}$$

and since the input is also a scalar (τ_j), R_j becomes

$$R_j = \eta_j \qquad j = 1, 2. \tag{91}$$

This results in $K_j(x)$ being a vector of the following form:

$$K_j(x) = [k_{j1} \;\; k_{j2} \;\; k_{j3} \;\; k_{j4} \;\; k_{j5} \;\; k_{j6}] \qquad j = 1, 2. \tag{92}$$

Replacing Q_j and R_j in Eq. (89) yields

$$A_j' P_j + P_j A_j - \frac{1}{\eta_j} P_j B_j B_j' P_j + C_{lj}' \mu_j C_{lj} = 0 \qquad j = 1, 2. \tag{93}$$

Choosing $\mu_1 = \mu_2 = 2$, and $\eta_1 = \eta_2 = \sqrt{2}$ will result in the matrices P_1 and P_2 (from Eq. (93)) being equal to:

$$P_1 = \begin{bmatrix} 6.90 & 0.14 & -0.05 & -0.01 & 0 & 0 \\ 0.14 & 0.06 & 0.01 & 0 & 0 & 0 \\ -0.05 & 0.01 & 1.39 & 0.01 & 0 & 0 \\ -0.01 & 0 & 0.01 & 0.01 & 0 & 0 \\ 0 & 0 & 0 & 0 & 10^{-3} & 0 \\ 0 & 0 & 0 & 0 & 0 & 2 * 10^{-5} \end{bmatrix} \tag{94}$$

$$P_2 = \begin{bmatrix} 3.93 & 0.14 & -0.10 & -0.01 & 0 & 0 \\ 0.14 & 0.03 & 0.01 & 0 & 0 & 0 \\ -0.10 & 0.01 & 0.72 & 2.8 * 10^{-3} & 0 & 0 \\ -0.01 & 0 & 2.8 * 10^{-3} & 2 * 10^{-3} & 0 & 0 \\ 0 & 0 & 0 & 0 & 5 * 10^{-4} & 0 \\ 0 & 0 & 0 & 0 & 0 & 10^{-5} \end{bmatrix} \tag{95}$$

Substituting these matrices into Eq. (87) for $R_j = \eta_j = \sqrt{2}$ gives the vectors K_{l1} and K_{l2} of the optimal feed-back gains:

$$K_{l1} = [-4.85 \;\; -1.99 \;\; -0.27 \;\; -2 * 10^{-3} \;\; 0 \;\; 0] \tag{96}$$

and

$$K_{l2} = [-4.83 \;\; -1.05 \;\; -0.25 \;\; -2 * 10^{-3} \;\; 0 \;\; 0] \tag{97}$$

Thus, the closed-loop state matrices $(A_1 - B_1 K_{l1})$ and $(A_2 - B_2 K_{l2})$ have the following poles for the first link,

$$s_{11,12} = -1.29 \pm 10.24i \qquad s_{13,14} = -2.90 \pm 52.65i \qquad s_{15,16} = -7.32 \pm 124.33i$$

and for the second link,

$$s_{21,22} = -2.48 \pm 10.06i \qquad s_{23,24} = -5.83 \pm 52.42i \qquad s_{25,26} = -7.32 \pm 124.40i$$

The first two pairs of poles for each link had their real part shifted further down the real axis (in comparison to the open-loop poles presented in section 4.2.1). The optimal control did not alter the third pole for each link since its contribution in the final response is negligible [2]. The imaginary parts of all the poles of the closed-loop transfer function were not affected by the optimal feed-back

gains, the aim of any control law being mainly to stabilise the system by shifting the real part of the appropriate poles into the negative half-plane. The outputs $u_{l1}(t)$ and $u_{l2}(t)$ can now be obtained according to the following equation:

$$u_{lj}(t) = C_{lj}\, e^{(A_j - B_j K_{lj})t} \underline{q}_{lj}(0) + u_{0lj} \qquad j = 1, 2. \tag{98}$$

$\underline{q}_{lj}(0)$ being the vector of initial conditions at the end-tip for the state variables of each link, u_{0lj} are the static deflections at the end-tip of each link. This last equation could be rewritten using the closed-loop poles as:

$$u_{lj}(t) = C_{lj}\, \mathcal{L}^{-1} \left\{ [s_{ji} I - A_j + B_j K_{lj}]^{-1} \right\} \underline{q}_{jl}(0) + u_{0lj} \qquad i = 1, 6;\ j = 1, 2. \tag{99}$$

the state number is indicated by the subscript i, the link number is indicated by the subscript j. $\mathcal{L}^{-1}$ relates to the inverse Laplace transform.

4.4 SIMULATION OF CONTROLLER PERFORMANCE

Figure 10 shows the time history of the end-tip deflection of the first and second link, respectively, with and without optimal control. It can be seen that the quadratic optimal control allows the links to vibrate freely as soon as the rotation is started. The manoeuver is operated very smoothly and as soon as the torques reach a certain magnitude (determined by the controller) they are automatically decreased (or increased if the link is in a braking phase). This effect of damping, caused by the torques, allows the suppression of the forced vibrations, and the controlled links are then subject to a free vibration. Therefore, the settling time is decreased enormously. The desired torques $\tau_1(t)$ and $\tau_2(t)$ are obtained by using Eq. (88) for both flexible links. They are then used to calculate the angles of rotation $\theta_1(t)$ and $\theta_2(t)$ of the rigid mode of both links by solving the following system of nonlineal differential equations:

$$\begin{bmatrix} \tau_1 \\ \tau_2 \end{bmatrix} = [D(\theta_1, \theta_2)] \begin{bmatrix} \ddot{\theta}_1 \\ \ddot{\theta}_2 \end{bmatrix} + [h(\theta_1, \theta_2, \dot{\theta}_1, \dot{\theta}_2)] + [c(\theta_1, \theta_2)] \tag{100}$$

This system of differential equations can be computed using the Matlab$^{(c)}$ package, where a programme based on Runge-Kutta method using $4th$ and $5th$ order functions can be relatively easily applied.

The input torque for the uncontrolled, then controlled first link is represented in Figure 11(a). The effect of the weighting parameter η_1 is obvious, since the torque derived from the quadratic optimal control law is smaller, but lasts almost as long as the torque applied without any control law. The acceleration and deceleration processes are controlled in such a way that less energy is dispersed. The rotation of the first rigid mode proceeds in two phases (Figure 11(b)), such that the end-tip of the first link maintains a continuous vibration (any sudden change of frequency is avoided by the controller).

In a similar manner, results concerning the torque for the second link and the angle of rotation of the rigid mode of the second link are shown in Figure 12. It can be seen from the time history of the controlled angle of rotation that the rigid body is rotated by -23.6 degrees in 0.64 seconds, then stopped for a small fraction of time, then the -30 degrees rotation is completed. However, the first phase of the rotation of the rigid body of the first link is carried out for 0.6 seconds only, which leads to a rotation of 20 degrees only (see Figure 11(b)). This is due to the fact that the important payload attached to the first link makes it more sensitive to vibration, thus the first phase of rotation is carried out in a slower manner.

On the other hand, the angles of rotation of the end-tip of the flexible body of both links (shown in Figure 13) give a quite different result from their rigid counterpart (Figures 11(b) and 12(b)). Nevertheless, the response associated with the links under a quadratic optimal control shows less vibrations and a faster settling time.

By comparing the angle of rotation of the end-tip of the first flexible link under quadratic optimal control (Figure 13(a)) to that obtained by the computed torque control (Figure 9(a)), it can be seen that the respective responses towards the end of the rotation are very similar (both control methods were effective in suppressing the residual vibrations), but towards the beginning of the rotation the torque designed according to the quadratic optimal control gives a faster response (during the first 0.6 seconds the computed torque gives a relatively delayed response).

The reason why both torques (designed according to both control techniques) produce the same effect towards the end of the rotation is that the rotation effected under quadratic optimal control is stopped at a certain stage to limit the energy produced by the torque (hence, limiting the current applied to the actuator of the link). This delay is found to be relatively equal to that produced at the start of rotation using computed torque control.

5 SUMMARY

The paper initially explained the necessity for having an accurate static and dynamic model of the two-flexible-link manipulator, which properly represents the coupling and interactions between the links. Such a model has been developed in previous work and the main steps involved in the construction of this model have been reviewed.

The functions to be fulfilled by the controller of a flexible manipulator system were outlined in section 1. Firstly, it must compensate for the static deflection of the flexible links under gravity forces and, secondly, it must act to reduce both the magnitude and time duration of link oscillations which arise naturally out of its flexibility. The paper has investigated the ability of two alternative controllers, a computed-torque controller and a quadratic optimal controller, to fulfill these functions. Simulation of their relative performance has shown that, whilst computed-torque control (which is essentially an open-loop method) can fulfill these functions to a limited extent, much better performance is obtained by the closed-loop, quadratic optimal controller.

REFERENCES

[1] Morris, A.S. and Madani, A., 1995, "Multi-Mode Modelling of a Flexible Link Robot Manipulator", *Robotics Research Group, Department of Automatic Control and Systems Engineering, The University of Sheffield, U.K.*, Research Report number 579, 1 June 1995. Submitted for publication in *Proc. I. Mech. E., Part I.*

[2] Morris, A.S. and Madani, A., 1995, "Static and Dynamic Modelling of a Two-Flexible-Link Robot Manipulator", Submitted for publication in *Robotica.*

[3] Timoshenko, S., Young, D.H. and Weaver, W.Jr., 1974, *Vibration Problems in Engineering.* Wiley. New York.

[4] Cannon, R.H.Jr. and Schmitz, E., 1984, "Initial Experiments on the End-Point Control of a Flexible One-Link Robot", *Int. J. Robotics Res.*, Vol. 3, no. 3, pp. 62-75.

[5] Morris, A.S. and Madani, A., 1995, "Inclusion of Shear Deformation Term to Improve Accuracy in Flexible-Link Robot Modelling", Submitted for publication in *Mechatronics.*

[6] Timoshenko, S. and Lessels, J.M., 1925, *Applied Elasticity*, First edition, Westinghouse Technical Night School Press.

[7] Tse, F.S., Morse, I.E. and Hinkle, R.T., 1978, "Mechanical Vibrations, Theory and Application", Second edition, Allyn and Bacon, Boston.

[8] Book, W.J., Maizza-Netto, O. and Whitney, D.E., 1975, "Feedback Control of Two Joint Systems with Distributed Flexibility", *ASME Journal of Dynamic Systems, Measurement and Control*, Vol. 97, pp. 424-431.

[9] Cannon, R.H. and Schmitz, E., 1984, "Initial Experiments on the Control of a Flexible Manipulator", *The International of Robotics Research*, Vol. 3, pp. 62-75.

[10] Fukuda, T., 1985, "Flexibility Control of Elastic Robot Arms", *Journal of Robotics Systems*, Vol.

2, no. 1, pp. 73-88.
[11] Meckl, P.H. and Steering, W.P., 1988, "Reducing Residual Vibration in Systems with Uncertain Resonances", *IEEE Control Systems Magazine*, Apr., pp. 73-76.
[12] Hyde, M. and Seering, W., 1991, "Inhibiting Multiple Mode Vibration in Controlled Flexible Systems", *Proceedings of 1991 American Control Conference*, Boston, MA, pp. 2449-2454.
[13] Luh, J.Y.S., Walker, M.W. and Paul, R.P., 1982, "Resolved Motion Force Control of Robot Manipulators", *ASME Journal of Dynamics Systems, Measurement, and Control*, Vol. 102, pp. 126-133.
[14] Pfeiffer, F., 1989, "A Feedforward Decoupling Concept for the Control of Elastic Robots", *Journal of Robotics Systems*, Vol. 6, no. 4, pp. 407-416.
[15] Asada, H., Ma, Z. and Tokumaru, H., 1990, "Inverse Dynamics of Flexible Robot Arms: Modeling and Computation for Trajectory Control", *ASME Journal of Dynamic Systems, Measurement and Control*, Vol. 112, pp. 177-185.
[16] Asada, H. and Stoline, J.J.E., 1986, *Robot Analysis and Control*, Wiley, New York, NY.
[17] Balas, M.J., 1978, "Feedback Control of Flexible Systems", *IEEE Transactions on Automatic Control*, Vol. AC-23, no. 4, pp. 673-679.
[18] Oakley, C.M. and Cannon, R.H., 1988, "Initial Experiments on the End-Point Control of a Two-Link Manipulator with a Very Flexible Forearm", *Proceedings of the 1988 American Control Conference*, Atlanta, GA, pp. 996-1002.
[19] Eisler, G.R., Robinett, R.D., Segalman, D.J. and Feddema, J.D., 1993, "Approximate Optimal Trajectories for Flexible-Link Manipulator Slewing Using Recursive Quadratic Programming", *Transactions of the ASME Journal of Dynamic Systems, Measurement, and Control*, Vol. 115, pp. 405-410.

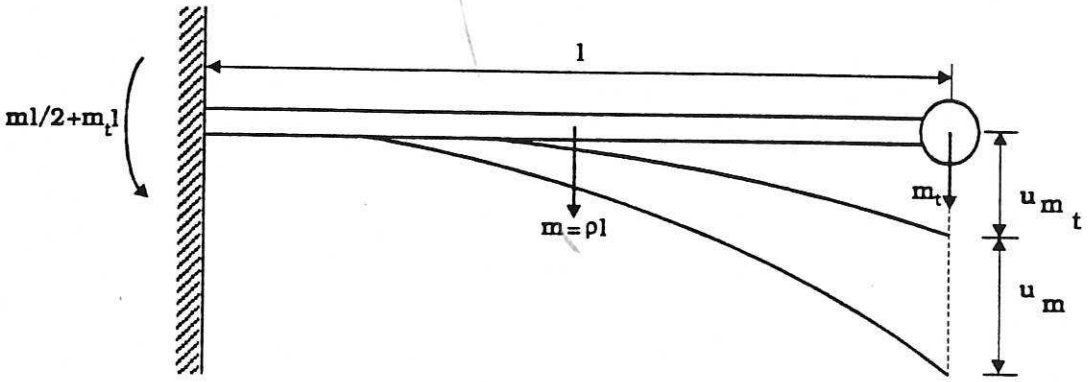

Figure 1(a) Deflection of a flexible link under the effect of its mass and payload.

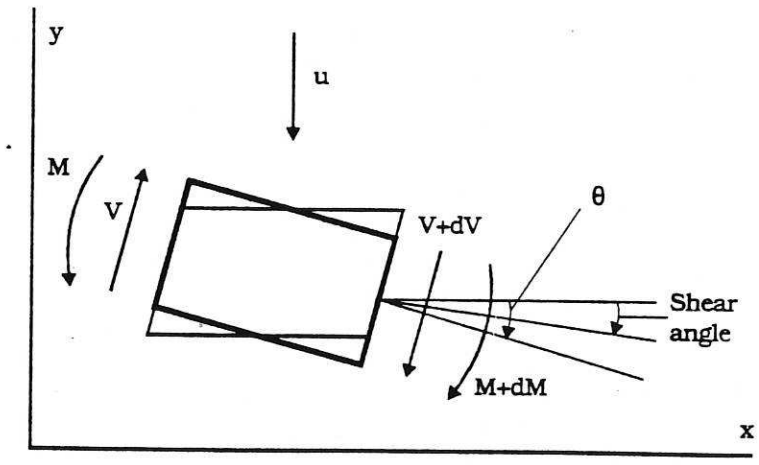

Figure 1(b) Lateral vibration of a beam with rotary inertia and shear deformation.

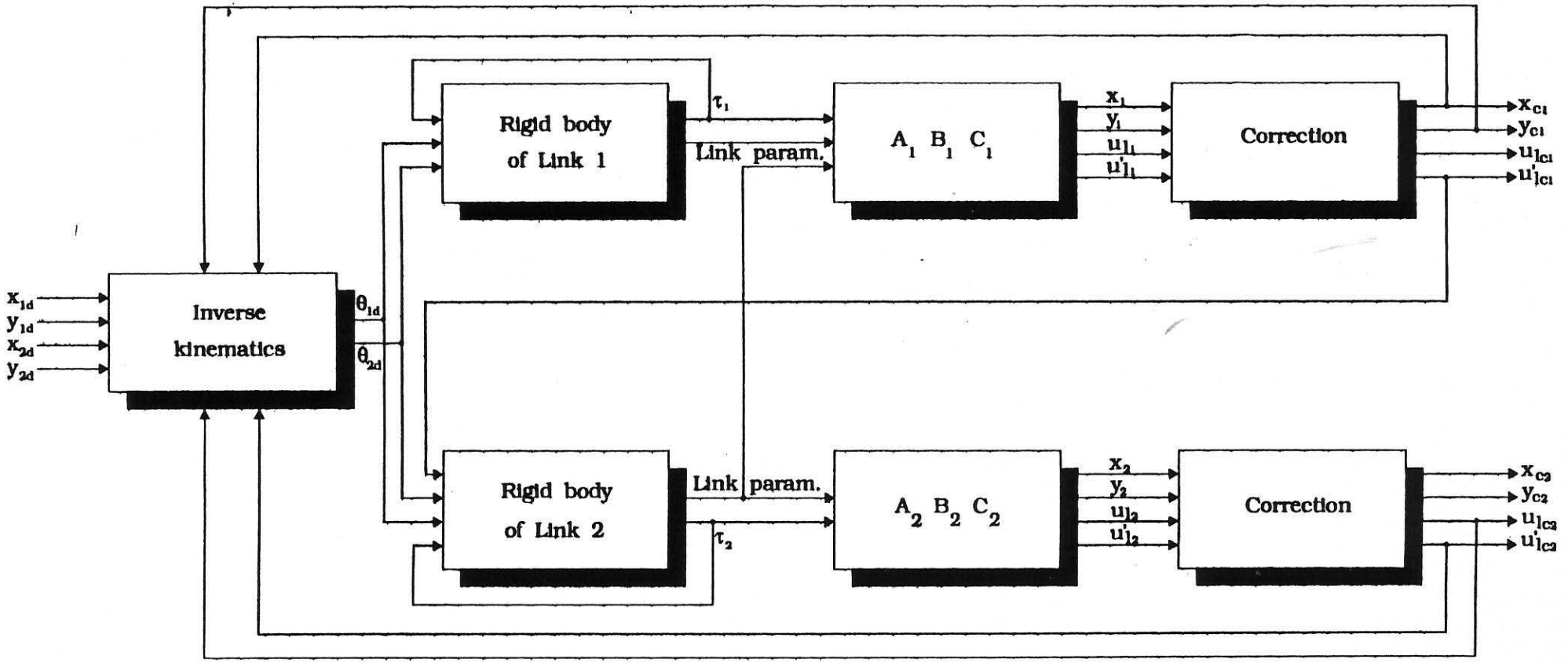

Figure 2 Block diagram of algorithm for modelling a two-link flexible manipulator.

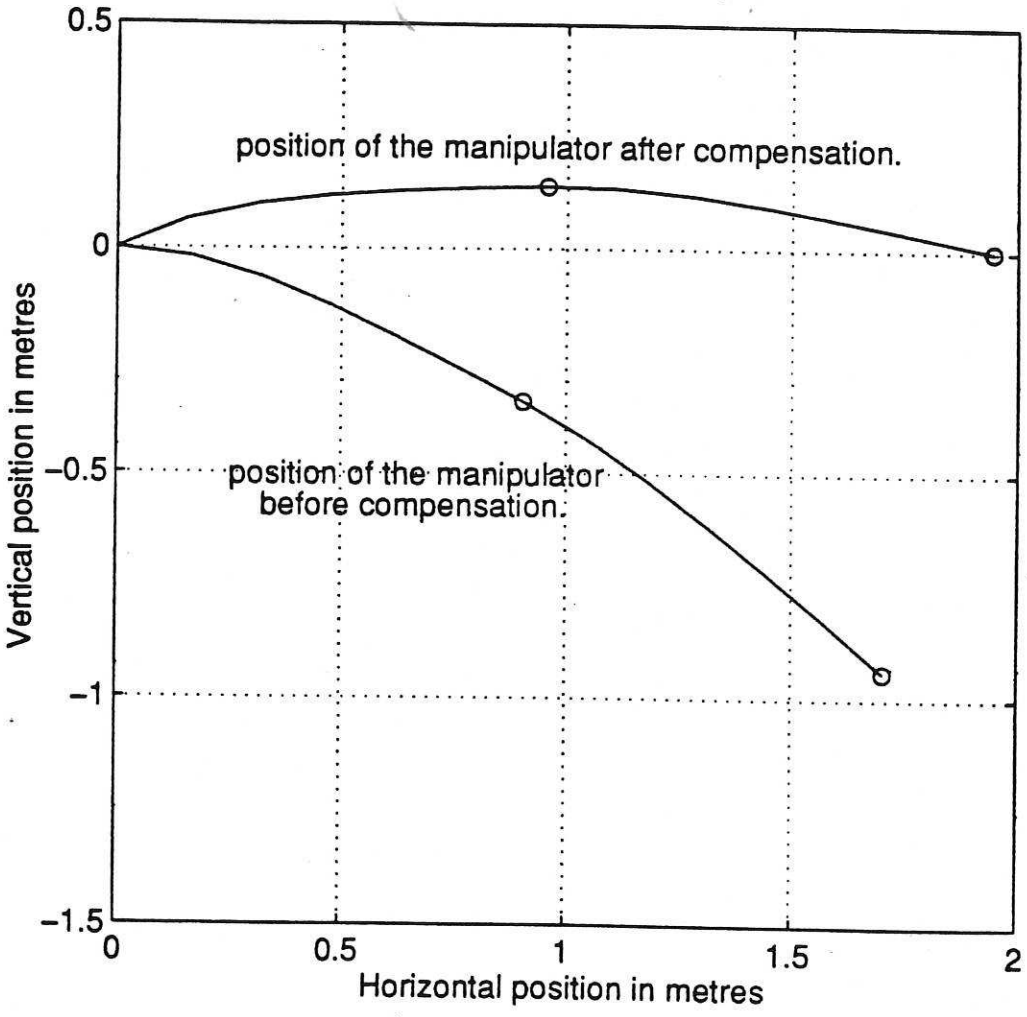

Figure 3. Compensation for the static deflection.

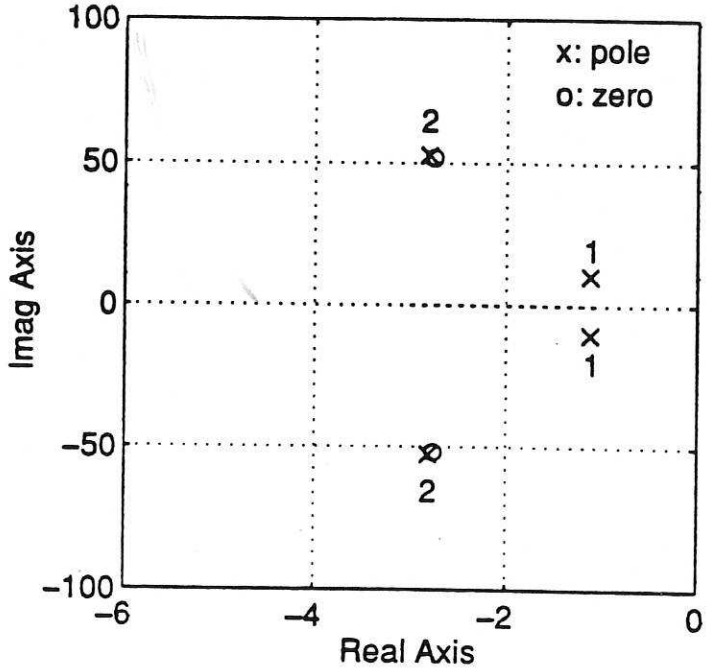

Figure 4(a). Root locus for the first flexible link.

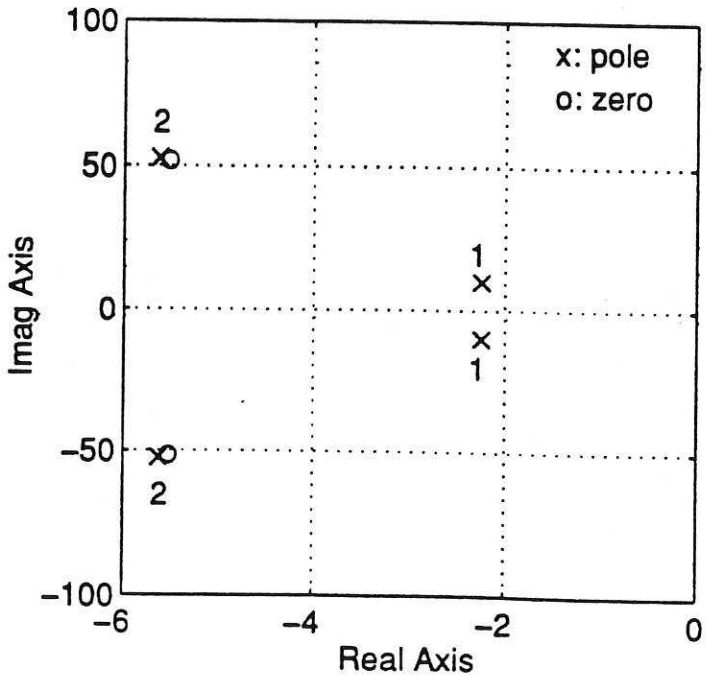

Figure 4(b). Root locus for the second flexible link.

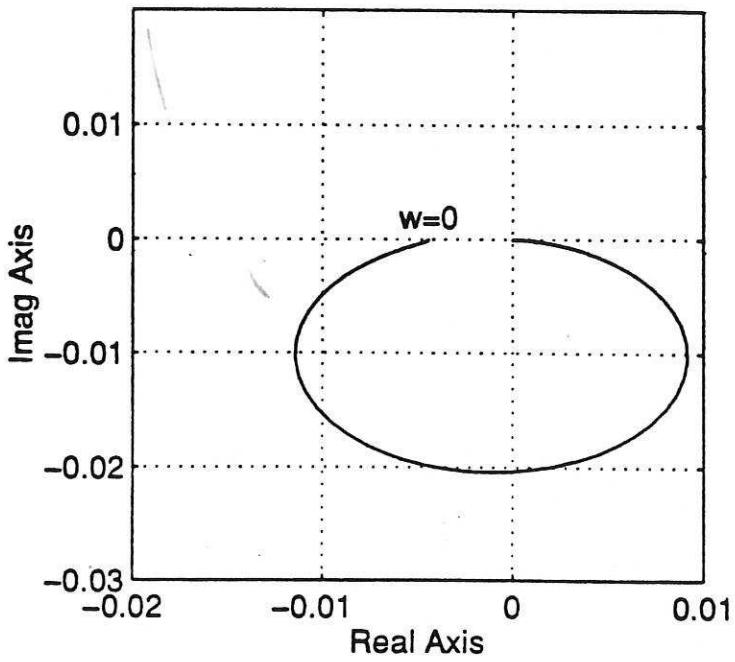

Figure 5(a). Nyquist diagram for the open−loop transfer function of the first elastic subsystem

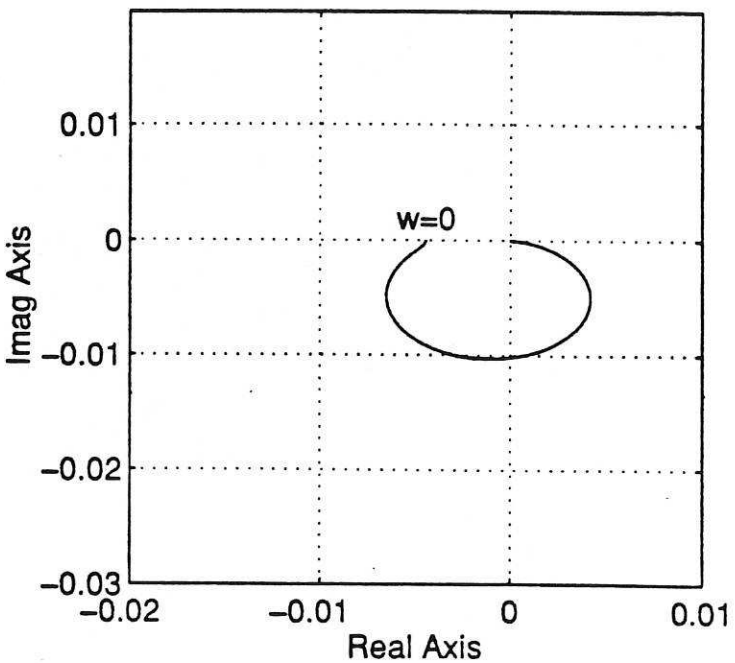

Figure 5(b). Nyquist diagram for the open−loop transfer function of the second elastic subsystem

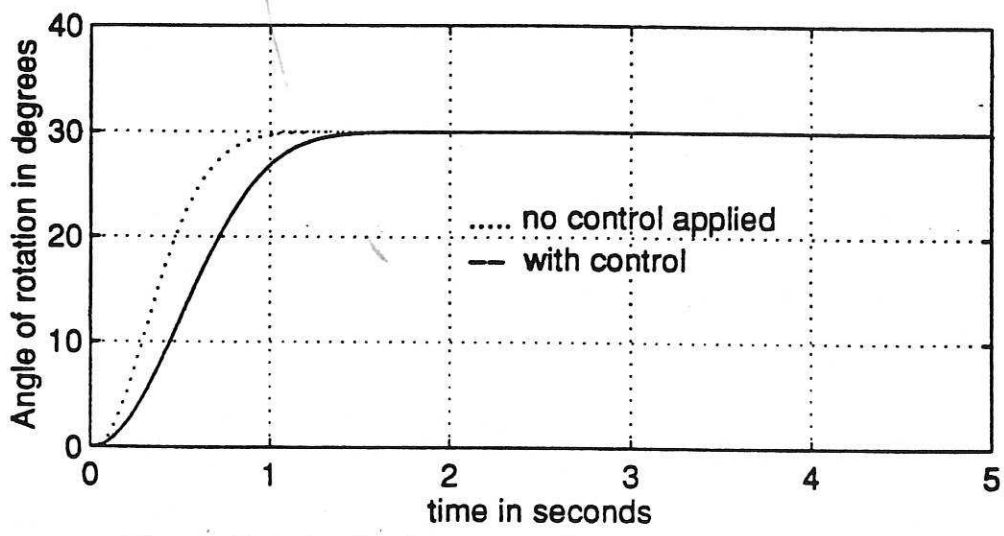

Figure 6(a). Angle of rotation of the rigid mode of link 1.

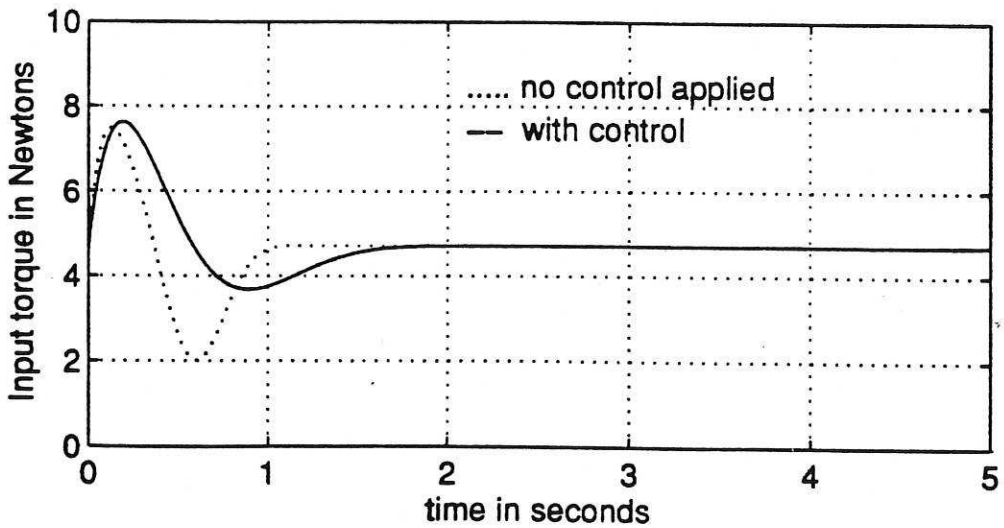

Figure 6(b). Input torque for the first flexible link.

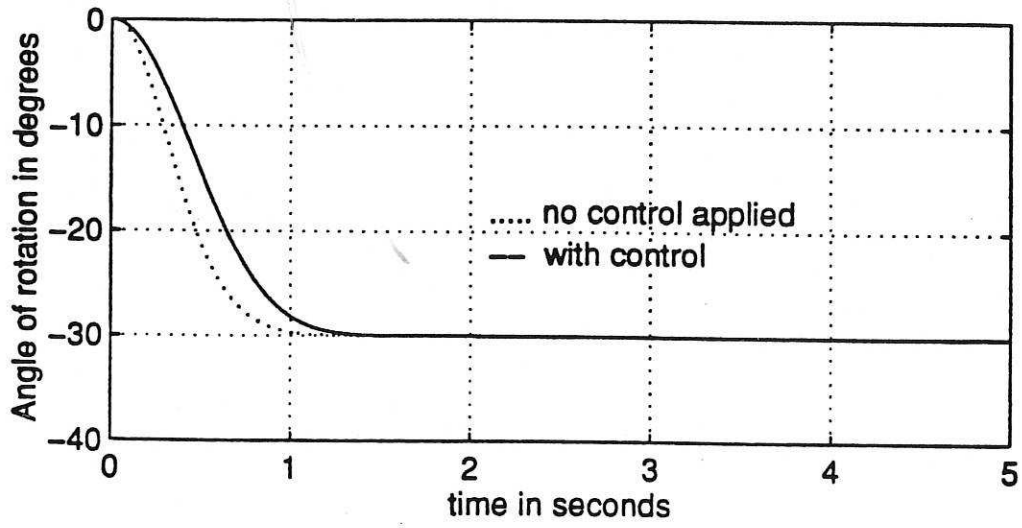

Figure 7(a). Angle of rotation of the rigid mode of link 2.

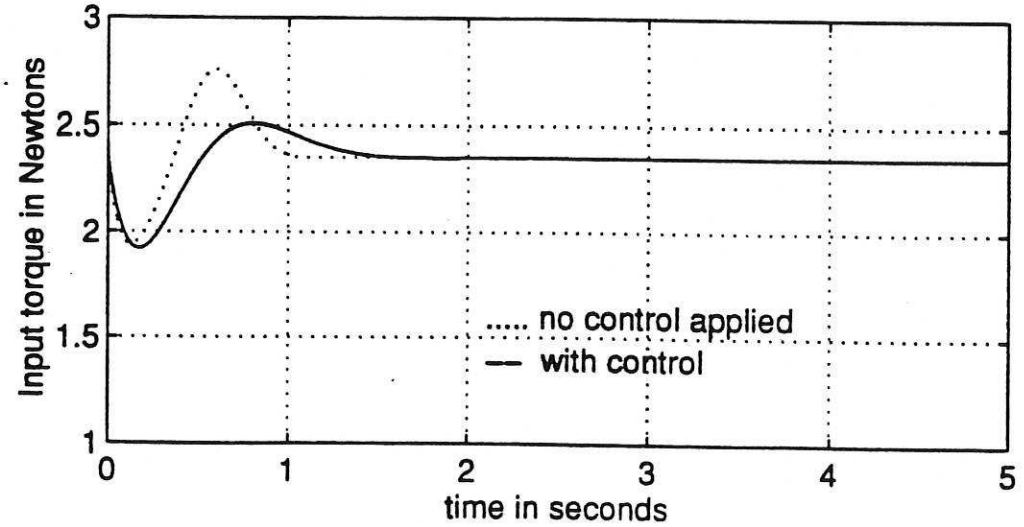

Figure 7(b). Input torque for the second flexible link.

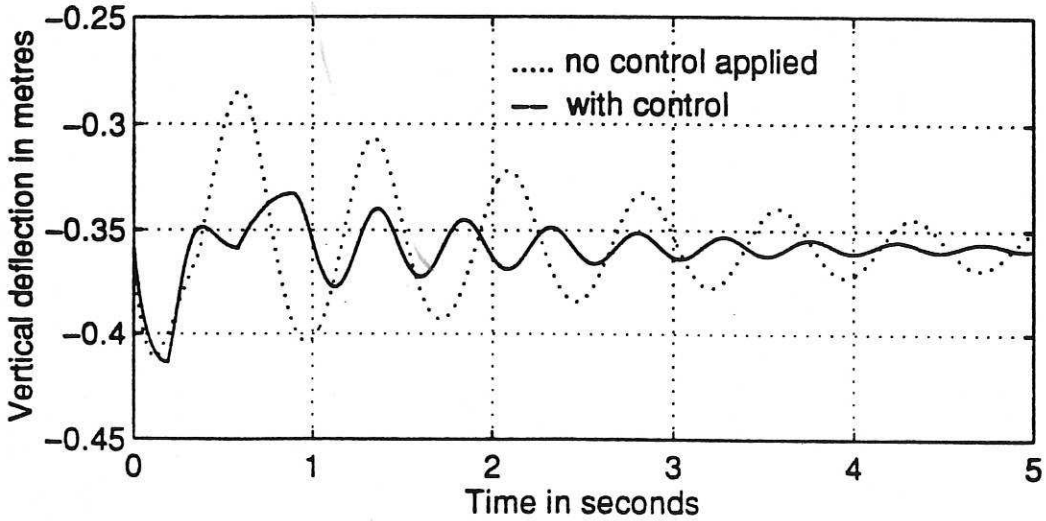

Figure 8(a). End–tip deflection of the first flexible link.

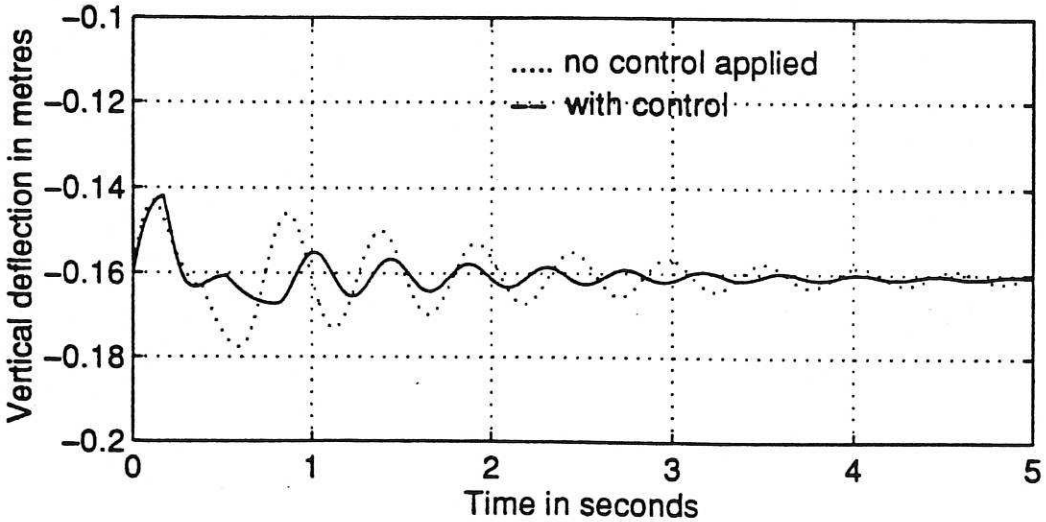

Figure 8(b). End–tip deflection of the second flexible link.

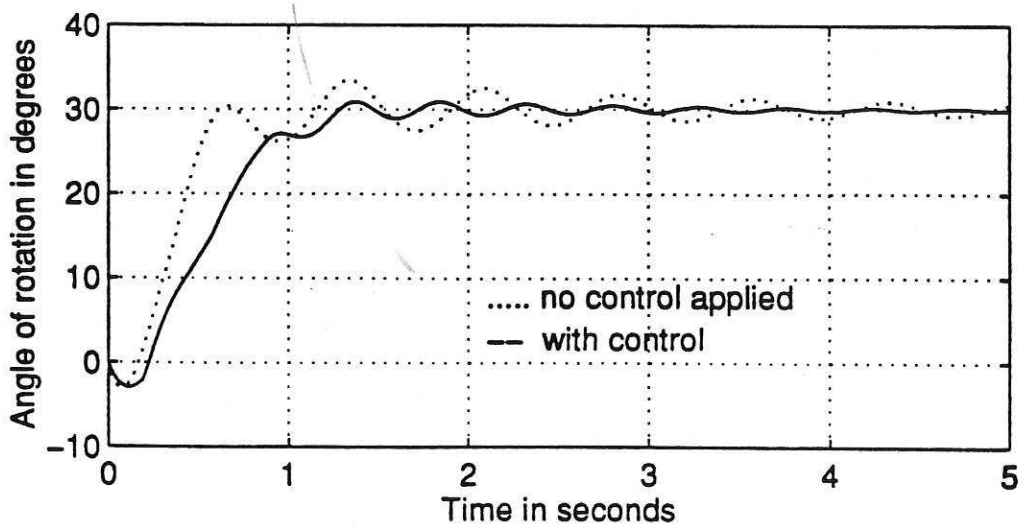

Figure 9(a). Angle of rotation of the end–tip of the first flexible link

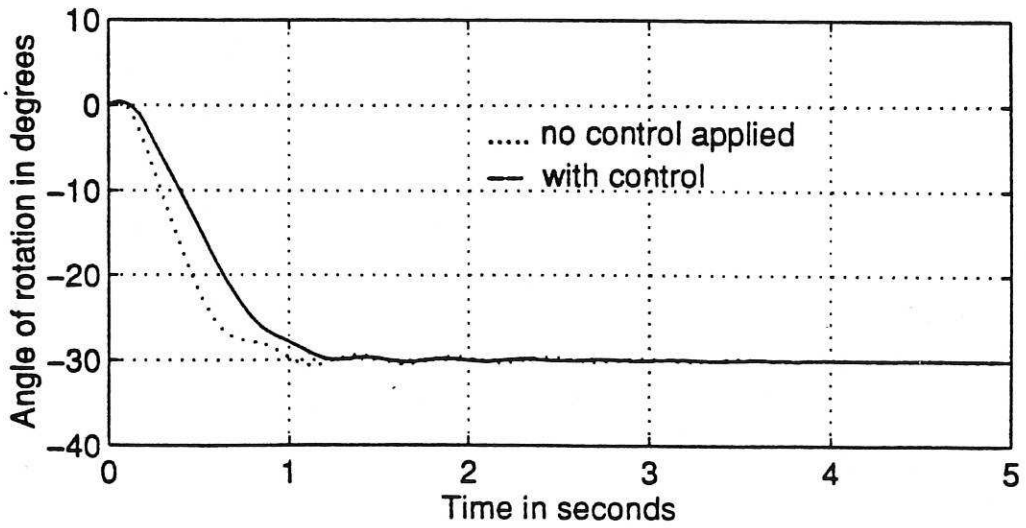

Figure 9(b). Angle of rotation of the end–tip of the second flexible link.

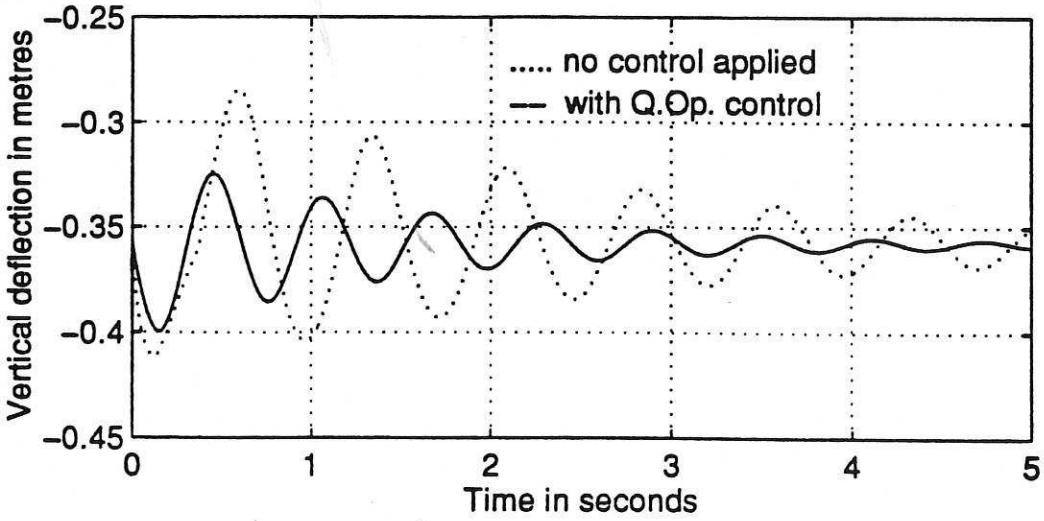

Figure 10(a). End–tip deflection of the first flexible link.

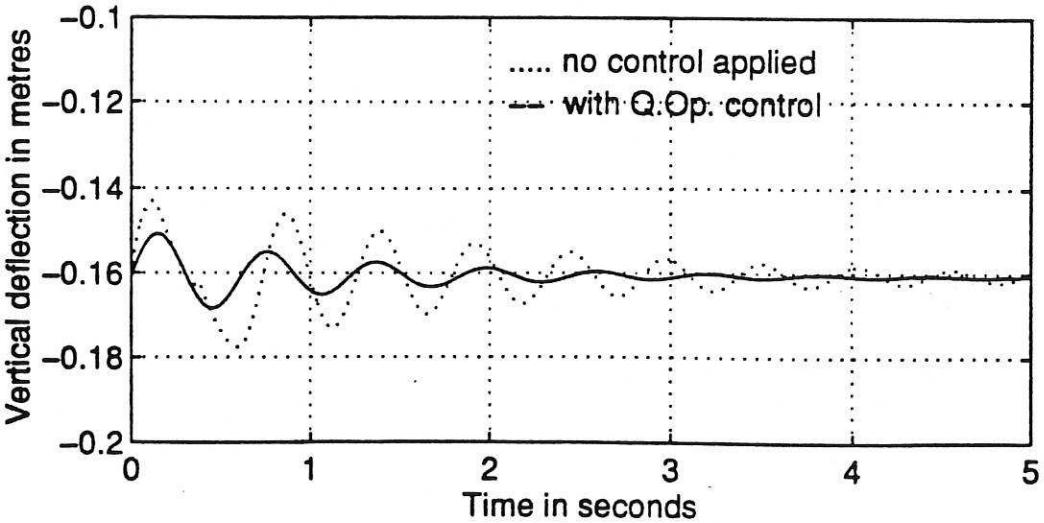

Figure 10(b). End–tip deflection of the second flexible link.

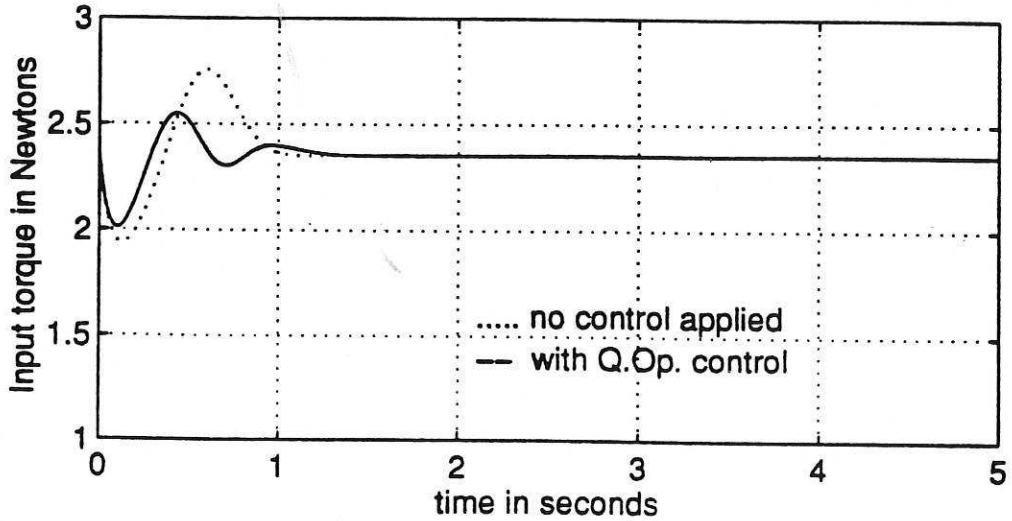

Figure 12(a). Input torque for the second flexible link.

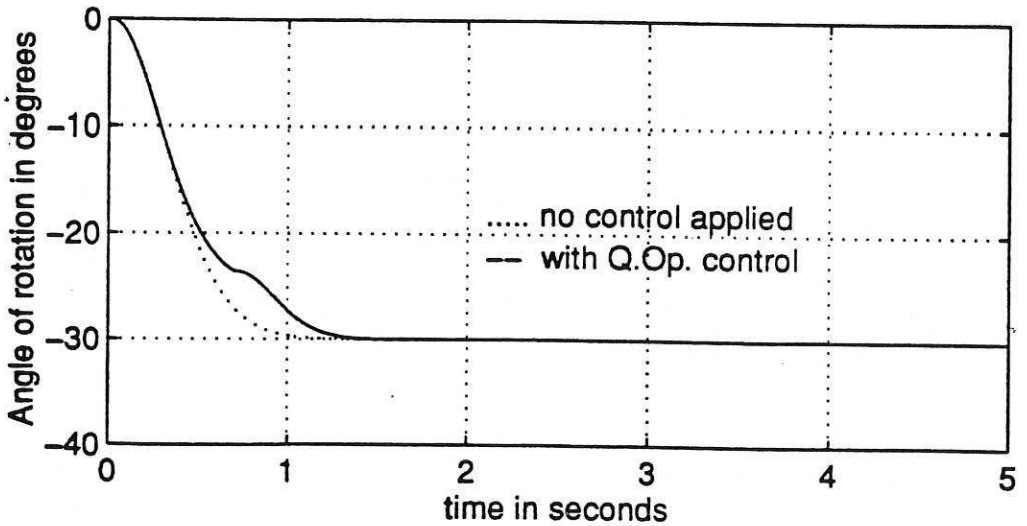

Figure 12(b). Angle of rotation of the rigid mode of link 2.